

Was the 2015 North Atlantic Subpolar Cold Anomaly Predictable?

ELIZABETH A. MAROON,^a STEPHEN G. YEAGER,^b GOKHAN DANABASOGLU,^b AND NAN ROSENBLUM^b

^a *Department of Atmospheric and Oceanic Sciences, University of Wisconsin Madison*

^b *National Center for Atmospheric Research, Boulder, Colorado*

(Manuscript received 25 September 2020, in final form 9 February 2021)

ABSTRACT: The subpolar North Atlantic (SPNA) experienced extreme cold during 2015, an event often called the “cold blob.” The evolution of this event in the Community Earth System Model version 1 Decadal Prediction Large Ensemble (CESM1-DPLE) hindcast initialized in November 2014 is compared to observations. This CESM1-DPLE hindcast failed to predict cold conditions during 2015 despite already cold SPNA initial conditions and despite having high sea surface temperature skill in the SPNA in all other years. The goal of this paper is to understand what led to this prediction failure in order to provide insight for future decadal prediction efforts. Our analysis shows that strongly positive North Atlantic Oscillation (NAO) conditions during winter and spring 2015 likely sustained the cold blob but were not simulated in any CESM1-DPLE members. We examine the rarity of the 2015 event using the CESM1-DPLE’s uninitialized counterpart, the CESM1 Large Ensemble (CESM1-LE). Results from the CESM1-LE indicate that the exceptional state of the observed NAO in the winter of 2015 is at least part of the explanation for why this event was not encompassed in the CESM1-DPLE spread. To test another possibility—namely, that deficiencies in the initial conditions degraded the prediction—we performed additional hindcasts using the CESM1-DPLE protocol but different initial conditions. Altering the initial conditions did not improve the simulation of the 2015 cold blob, and in some cases, degraded it. Given the difficulty of predicting this event, this case could be a useful test bed for future prediction system development.

KEYWORDS: North Atlantic Ocean; Climate prediction; Hindcasts; Climate models

1. Introduction

The skill of interannual-to-decadal climate predictions has increased considerably over the last decade, which, given the relevance of these time scales to decision-making, is of great interest to stakeholders (e.g., Meehl et al. 2009; Kirtman et al. 2013; Smith et al. 2019). Multiyear skill has been demonstrated for impacts ranging from Atlantic hurricanes and sea ice loss to ocean acidification and terrestrial carbon fluxes (Smith et al. 2007, 2010; Yeager et al. 2012, 2015; Lovenduski et al. 2019; Brady et al. 2020). While warming associated with greenhouse gas emissions is responsible for much of the prediction skill on lead times longer than a few years, initialization near the observed climate state contributes significant additional skill, especially in the subpolar North Atlantic (SPNA) (van Oldenborgh et al. 2012; Meehl et al. 2014; Yeager et al. 2018). By setting a model’s initial state near to that observed, the predicted trajectory is more likely to follow the observed trajectory beyond the effects of persistence alone.

Much effort to improve initial value predictability on interannual-to-decadal time scales has focused on the SPNA, where ocean heat convergence influences climate remotely through communication by the coupled atmosphere–ocean system (Griffies and Bryan 1997; Collins et al. 2006; Keenlyside et al. 2008; Msadek et al. 2010; Robson et al. 2012; Danabasoglu et al. 2016). This expectation for low-frequency predictability

stemming from subpolar processes is built on a thoroughly examined narrative that connects high-frequency atmospheric forcing [often associated with the North Atlantic Oscillation (NAO)] to Atlantic multidecadal variability (AMV) in sea surface temperature (SST) (e.g., Delworth et al. 2017; Kim et al. 2020, and references therein). In winter, the fast SST response (i.e., weather-to-seasonal time scales) to anomalously strong SPNA wind forcing has a tripole pattern (Marshall et al. 2001; Visbeck et al. 2003). In response to positive NAO winds, the tripole pattern has cooling in the Labrador Sea and western subpolar gyre region due to both turbulent heat fluxes and Ekman advection (Deser et al. 2010). Multiple years of positive NAO forcing lead to deep convection and a later strengthening of the Atlantic meridional overturning circulation (AMOC) and subpolar gyre (Curry et al. 1998; Delworth and Dixon 2000; Eden and Willebrand 2001; Latif et al. 2006; Danabasoglu 2008; Danabasoglu et al. 2012; Yeager and Danabasoglu 2014; Delworth and Zeng 2016). As a result of strengthened ocean circulation, subpolar ocean heat convergence increases, leading to increased subpolar ocean heat content (OHC) and SST (Delworth et al. 1993; Latif et al. 2004; Knight 2005; Zhang and Zhang 2015; Wills et al. 2019). A low sea level pressure (SLP) anomaly in the SPNA forms in response to the increased SST; by weakening trade winds, the atmospheric response transmits the high SST anomaly from the SPNA to the subtropics and tropics via air–sea coupling and low cloud feedbacks, leading to a basin-scale positive SST anomaly with a multidecadal time scale (Visbeck et al. 2003; Li et al. 2013; Brown et al. 2016; Kim et al. 2020). Societally relevant climate impacts follow from positive AMV anomalies, including increased Sahel precipitation, Atlantic hurricane activity, and European temperature and precipitation, among many other impacts (Folland et al.

 Denotes content that is immediately available upon publication as open access.

Corresponding author: Elizabeth A. Maroon, emaroon@wisc.edu

DOI: 10.1175/JCLI-D-20-0750.1

© 2021 American Meteorological Society. For information regarding reuse of this content and general copyright information, consult the [AMS Copyright Policy](#) (www.ametsoc.org/PUBSReuseLicenses).

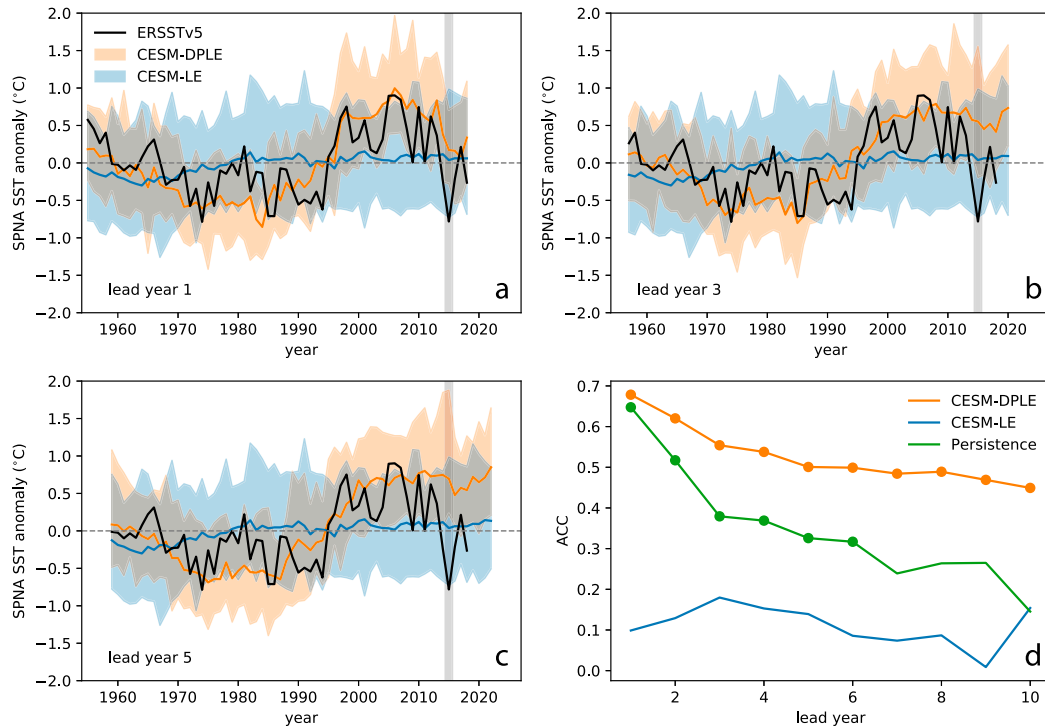


FIG. 1. Annual mean SPNA SST predictions for lead years (a) 1, (b) 3, and (c) 5, and (d) the SPNA SST anomaly correlation coefficient (ACC). Ensemble mean (dark lines) and range (light shading) are shown for both the CESM1-DPLE (orange) and CESM1-LE (blue). The observed SPNA SST from ERSSTv5 (Huang et al. 2017) is shown in black. The ACC of ensemble mean anomalies with observed anomalies is shown for the CESM1-DPLE (orange), CESM1-LE (blue), and persistence forecast (green); ACC significant at the 95% level is indicated by circles. SPNA is defined here as 45° – 20° W, 45° – 60° N; see the box in Fig. 4a.

1986; Enfield et al. 2001; Goldenberg et al. 2001; Lu et al. 2006; Knight et al. 2006; Zhang and Delworth 2006; Sutton and Dong 2012; Zhang et al. 2019). On shorter, decadal time scales, subpolar and basin-scale North Atlantic SST anomalies have also been attributed to wind forcing via Gulf Stream excursions and expansion or contraction of the subpolar gyre (e.g., Piecuch et al. 2017; Nigam et al. 2018). In summary, a narrative in the literature suggests that initializing a climate model with an Atlantic Ocean state that has the imprint of prior wind forcing should lead to prediction skill for up to 10 or more years in the SPNA and beyond.

Multyear predictions from many models do indeed show high skill in the SPNA region and associated climate impacts (García-Serrano and Doblas-Reyes 2012; Kim et al. 2012; Robson et al. 2012; Yeager et al. 2012; van Oldenborgh et al. 2012; Chikamoto et al. 2013; Doblas-Reyes et al. 2013; Msadek et al. 2014; Scaife et al. 2014; Bellucci et al. 2015; Yeager et al. 2015; Smith et al. 2019). Skillful prediction of high-frequency SPNA SST evolution, however, has not been demonstrated. The Community Earth System Model version 1 Decadal Prediction Large Ensemble (CESM1-DPLE)—the initialized hindcasts used in the present study—fits this characterization (Yeager et al. 2018; Yeager 2020). It has high SPNA SST and OHC skill on low frequencies that can be attributed to initialization, but fails to capture large year-to-year SST fluctuations

(Figs. 1 and 2). The CESM1-DPLE's SPNA SST skill exceeds that expected from external forcing alone, which is quantified by using the CESM1 Large Ensemble (LE) as uninitialized predictions (Kay et al. 2015). The observed SPNA (here defined as 45° – 20° W, 45° – 60° N) SST is indicated by the black line in Figs. 1a–c. The CESM1-LE has low and insignificant anomaly correlation coefficient (ACC) for SPNA SST in all lead years (blue, Fig. 1d). In contrast, the CESM1-DPLE (orange), does have significant ACC that exceeds the persistence prediction (green line) for all 10 lead years. There is, however, a notable exception to the CESM1-DPLE's subpolar skill: observed 2015 SPNA SST falls below the CESM1-DPLE spread for all ensemble hindcasts that include a prediction for 2015, even for the hindcast initialized only a few months prior in November 2014 (i.e., Fig. 1a at 2015). Not only is the CESM1-DPLE spread insufficient to encompass this 2015 “cold blob,” but the ensemble mean anomaly is also positive during this near-record cold event. The failure is also present in upper OHC (see Fig. ES3 in Yeager 2020), indicating that the issue extends to the upper ocean.

Determining why the CESM1-DPLE failed to predict the 2015 cold blob has importance beyond understanding a single case: we expect that forecast errors early in a simulation lead to forecast errors at later times. In the SPNA of the CESM1-DPLE, this premise appears valid. Lead year 1 forecast errors in SPNA SST are associated with later forecast errors (Fig. 2a)

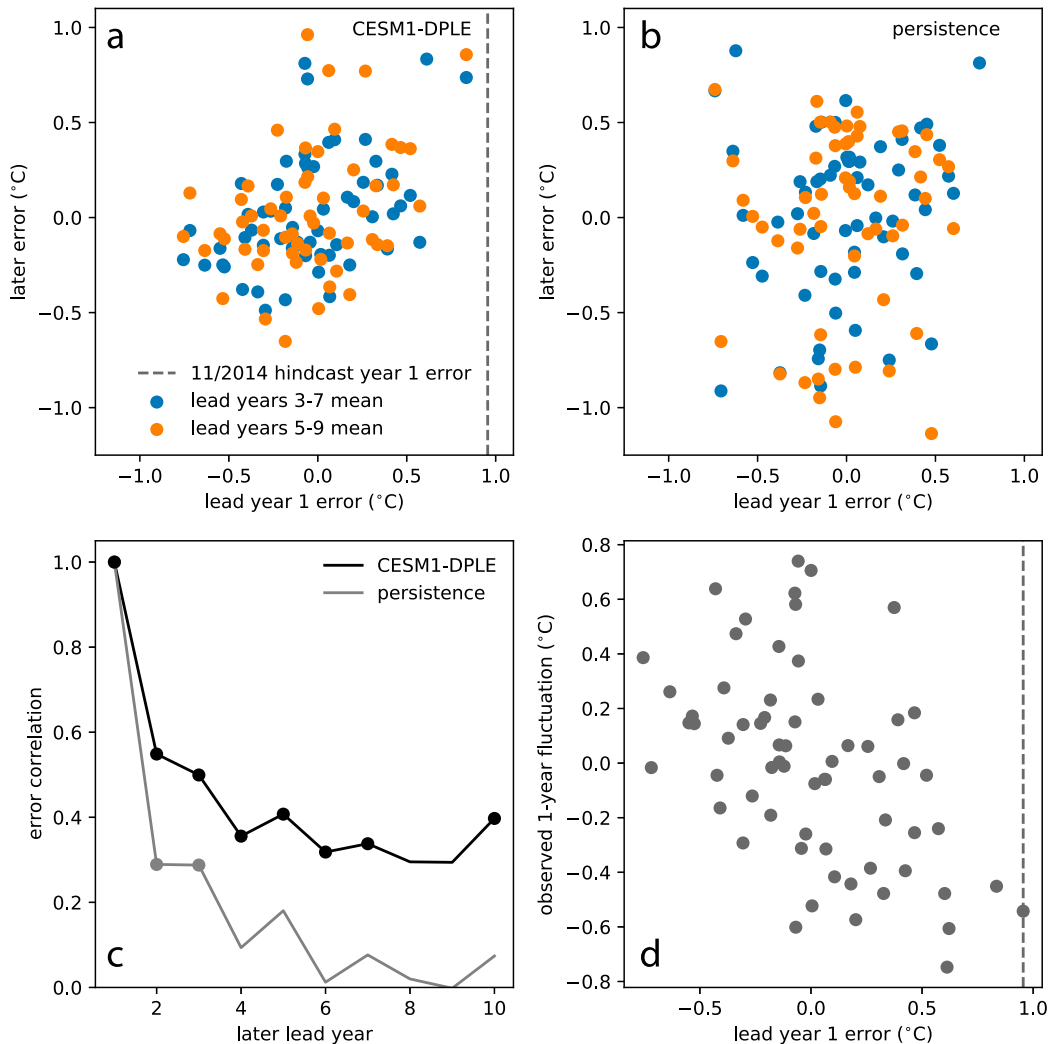


FIG. 2. Scatterplot of SPNA SST lead year 1 errors with later errors from the (a) CESM1-DPLE and (b) persistence hindcasts. Lead year 1 errors are on the x axis, while later errors are on the y axis, and each circle indicates the ensemble mean from an individual hindcast. Errors plotted are the difference between CESM1-DPLE ensemble mean or persistence forecast and the observed SPNA SST from ERSSTv5. Later errors for the lead year 3–7 mean (blue) and 5–9 mean (orange) are shown. (c) Correlation of lead year 1 error with the error from later individual lead years for the CESM1-DPLE (black) and persistence (gray), with circular markers indicating 95% significant correlations. (d) Lead year 1 error plotted against observed 1-yr fluctuations. The observed year 1 error for the November 2014 hindcast is indicated by the dashed line in (a) and (d).

with correlations of $R = 0.44$ and $R = 0.36$ for errors averaged over lead years 3–7 and 5–9, respectively. Both correlations are significant above 95% confidence using a two-tailed Wald test with the t distribution, which is the significance level and test used in all following correlations. This relationship is not an artifact of the 5-yr averaging; lead year 1 error is also significantly correlated with the later error from all lead years except years 8 and 9 where the cutoff for 95% significance is only barely missed (black line, Fig. 2c). Persistence alone does not explain the relationship (Fig. 2b): for the persistence forecast, the correlation between lead year 1 error and later error is weak for 5-yr averages ($R = 0.15$ and $R = 0.05$ for lead years

3–7 and 5–9 respectively) and for individual lead years after year 3 (gray line, Fig. 2c). The correlation of later errors with lead year 1 errors is always greater in the CESM1-DPLE than the persistence forecast. These results together indicate that SPNA SST error that develops in the first year of simulation actively influences the forecast beyond the effects of error persistence. The case investigated here—the 2015 cold blob—is associated with the largest lead year 1 error in SPNA SST in the entire CESM1-DPLE (dashed gray line, Fig. 2a), suggesting that SPNA evolution in the November 2014 hindcast will also have particularly high error through 2024. The CESM1-DPLE has difficulty predicting fast changes in SPNA

SST, as occurred from 2014 to 2015. Lead year 1 SPNA SST error is correlated ($R = -0.49$) with the observed 1-yr SPNA SST fluctuation (Fig. 2d). The observed 2015 fluctuation in SPNA SST is the fifth largest during the period covered by the CESM1-DPLE (1955–2018). Because the CESM1-DPLE is generally unable to predict sharp 1-yr fluctuations, successful prediction of the 2015 cold blob may have been difficult for this reason alone. Although prediction studies in the SPNA have focused on low-frequency modes (often related to the AMOC), the issues described above suggest that more attention on the initial high-frequency evolution and its influence on longer time scale predictions is needed (see, e.g., [Tietsche et al. 2020](#)). Understanding what went wrong in this specific cold blob case may shed light on how to improve future iterations of seasonal-to-multiyear CESM predictions.

Before we investigate why the CESM1-DPLE did not predict the cold blob, a brief summary of the observed event is first required. External forcing, low-frequency (multidecadal) variability, and high-frequency atmospheric forcing (weather) all likely contributed to the evolution of the 2015 SPNA cold blob ([Duchez et al. 2016](#); [Yeager et al. 2016](#); [Josey et al. 2018](#)). On multidecadal and longer time scales, SPNA cooling is likely caused by some combination of radiative forcing and low-frequency ocean variability ([Drijfhout et al. 2012](#); [Terray 2012](#); [Rahmstorf et al. 2015](#); [Robson et al. 2016](#)). In global warming projections, SPNA cooling has a “warming hole” pattern in response to radiative forcing, while multidecadal AMOC internal variability tends to be associated with a broader subpolar-wide cooling or warming (e.g., [Wills et al. 2019](#)). Although both decadal and multidecadal processes likely contributed to a cold background environment more conducive for a SPNA cold extreme (e.g., [Piecuch et al. 2017](#); [Årthun et al. 2021](#)), the majority of the SPNA cooling for the 2015 cold blob occurred rapidly, starting in 2013 due to high-frequency atmospheric forcing ([Grist et al. 2016](#); [Duchez et al. 2016](#); [Yeager et al. 2016](#); [Josey et al. 2018](#)). From 2013 to 2015, the annual mean SPNA SST dropped more than 1°C (Fig. 1a) and was associated with strong surface heat loss to the atmosphere. In 2014 heat loss was associated with the strongest winter mean east Atlantic pattern (EAP) since 1950, enhanced subpolar mode water formation, and a cold anomaly that extended down to 1000 m ([Grist et al. 2016](#); [Josey et al. 2018](#)). This cold anomaly at depth preconditioned the SPNA for further temperature reduction in early 2015 when strong winter NAO conditions persisted ([Duchez et al. 2016](#); [de Jong and de Steur 2016](#); [Josey et al. 2018](#)). After strong cooling, the anomaly reached maximum amplitude during summer of 2015 (Fig. 3a) before weakening. By summer, its presence likely contributed to the summer 2015 European heat waves, a societally relevant impact that further emphasizes the need to thoroughly understand the 2015 cold blob ([Duchez et al. 2016](#); [Mecking et al. 2019](#)). Interestingly, the SPNA cold blob formed along with rapidly freshening conditions, and is partly collocated with a fresh blob. [Holliday et al. \(2020\)](#) show that this freshening occurred from 2010 onward and amplified from 2012–16 due to forcing by positive NAO and positive EAP conditions reorganizing ocean freshwater transport.

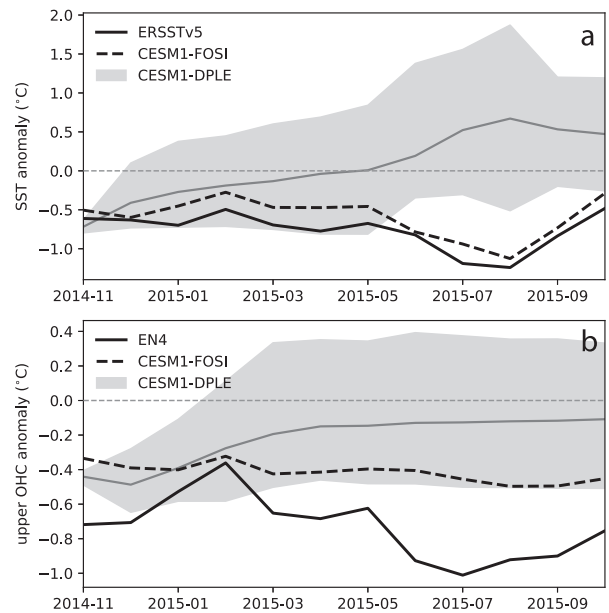


FIG. 3. Evolution of (a) SPNA SST and (b) upper 300-m OHC anomalies with respect to the CESM1-DPLE lead-time varying climatology. The observed SST and OHC (here indicated by volume-mean temperature) from ERSSTv5 and EN4 respectively are indicated by the black solid lines. CESM1-FOSI output is shown by the dashed black line and the CESM1-DPLE ensemble mean prediction and minimum-to-maximum range are shown by the grey line and shading.

The goal of our study is to understand why the CESM1-DPLE did not predict the 2015 cold blob. After introducing the CESM1-DPLE and other associated simulations and methods in section 2, the observed and predicted evolution of the 2015 cold blob in the CESM1-DPLE predictions is described in section 3. From there, we test a number of hypotheses that might explain why the cold blob was not predicted. In section 4 we present some implications of our findings, and finally we summarize our results in section 5.

2. Methods and datasets

The predictions examined here are from the CESM1-DPLE, a large ensemble of initialized hindcasts and forecasts ([Yeager et al. 2018](#)). The CESM1-DPLE consists of 122-month-long, 40-member ensembles initialized on 1 November each year from 1954 through 2017. Because our study is on the 2015 cold blob, the hindcast initialized on 1 November 2014 is the focus. The external forcing (e.g., greenhouse gases, solar forcing, aerosols, etc.) and the CESM version used are identical to that in the CESM1-LE ([Kay et al. 2015](#)). The CESM1-LE can thus be used as an uninitialized counterpart to the CESM1-DPLE; comparing against the CESM1-LE quantifies how much of the prediction skill is from external forcing versus initial conditions (ICs). Ocean and sea ice ICs are the full fields from a CESM1 Forced Ocean and Sea Ice (FOSI) simulation driven by CORE (Coordinated Ocean-Ice Reference Experiments; [Large and](#)

TABLE 1. Description of hindcasts.

Hindcast	Members	Description
CESM1-DPLE	40 members	The set of CESM1 initialized prediction hindcasts described in Yeager et al. (2018)
CESM1-LE	40 members	The large ensemble of Kay et al. (2015), used here as an uninitialized counterpart to the CESM1-DPLE. The CESM1-DPLE and LE share model codebase and boundary forcings.
CESM1-DPLE extension	20	Additional ensemble members added to the November 2014 CESM1-DPLE hindcast
Nov-Ice	10	Atmospheric ICs from CESM1-LE #34 1 November 2014 to induce more rapid B-K sea ice formation
Climo-Init	10	Ocean and sea ice ICs derived from CESM1-LE #34 1 Nov climatology (1954–2005)
EN4-Anom-Init	20	Ocean temperature and salinity IC anomalies from EN4 are added to CESM1-LE climatology. Sea ice ICs use CESM1-LE 1 Nov climatology (1954–2005).
ERA-IC	10	All atmospheric IC fields from ERA-Interim reanalysis

Yeager 2009) forcing.¹ Fields from the CESM1-FOSI simulation are also compared to the CESM1-DPLE predictions for mechanistic comparison. CESM1-DPLE atmosphere and land ICs are from the CESM1-LE ensemble member 34 restart files of the same date as the initialization date; this ensemble member is the only one available with the necessary November restart files available for each year. In the CESM1-DPLE and all additional hindcasts presented here, spread in the ensemble members is created by adding random round-off level perturbations of order 10^{-14} K to the full field of atmospheric temperature ICs, as in Kay et al. (2015).

Because the CESM1-DPLE uses a full-field initialization approach, hindcasts drift toward model climatology. A lead-time dependent drift removal method is used to extract climate anomalies, as described in Kim et al. (2012), Doblas-Reyes et al. (2013), Yeager et al. (2018), and others. For raw output Y_{jrm} from ensemble member m initialized in year j at lead time τ , the anomaly Y'_{jrm} is calculated by subtracting $\langle Y_{\tau} \rangle$. Brackets and overbars indicate means over ensemble members and initialization years, respectively. To calculate $\langle \bar{Y}_{\tau} \rangle$, which represents a drifting climatology, only output that falls on or between January 1964 and December 2014 is used, as in Yeager et al. (2018).

To investigate why the cold blob was not predicted, we conduct additional hindcast experiments with each set deviating in one way from the CESM1-DPLE protocol (see Table 1). Because we are focusing on the first 14 months of evolution, all hindcasts are initialized on 1 November 2014 and extend through 31 December 2015.

a. CESM1-DPLE extension

The first additional hindcast is a 20-member extension of the November 2014 CESM1-DPLE hindcast—increasing the ensemble size to 60—to test the effects of ensemble size on the range of forecasts.

¹ Standard CORE forcing is used everywhere except in the tropics where CORE winds are blended with those from NOAA's Twentieth Century Reanalysis (Compo et al. 2011) before 2010 and JRA55-do (Tsujino et al. 2018) after 2010 to ameliorate tropical Pacific initialization shock. See Yeager et al. (2018).

b. Nov-Ice

This experiment is designed to test the influence of having too little sea ice in the Barents–Kara (B-K) Seas compared to observations during November 2014. These 10 ensemble members use atmospheric ICs that favor the production of sea ice during November 2014. As will be shown below, the sea ice deficiency in the original CESM1-DPLE hindcast is due to the original atmospheric ICs from CESM1-LE #34 restart on 1 November 2014. New atmospheric ICs are from the 1 November 2004 restart file from CESM1-LE #34, which was chosen for its atmospheric circulation that should promote more rapid November ice formation in the B-K Seas.

c. EN4-Anom-Init and Climo-Init

The next set of hindcasts are used to test the potential impact of errors in the CESM1-FOSI ocean state of November 2014, by using ICs from an observation-based gridded analysis in an anomaly-initialization approach. Raw observation-based ocean fields are likely far from the CESM1's attractor and their use as ICs may cause a nonphysical shock during the beginning of the simulation. Avoiding shock is one reason for the full-field initialization approach from the CESM1-FOSI, which despite the surface boundary forcing likely has a climatology close to that of the fully coupled CESM1. Anomaly initialization, another strategy to avoid such shocks, uses ICs constructed from the fully coupled CESM1 climatology and observation-based ocean anomalies. We first create a hindcast of 10 ensemble members where the 1 November 2014 ocean and sea ice ICs are replaced with the CESM1-LE 1 November climatology (Climo-Init). The climatology is constructed from the CESM1-LE member 34's 1 November restart files from 1954 to 2005. All other ICs are the same as those used in the CESM1-DPLE protocol. We found that 10 ensemble members were sufficient to produce a stable ensemble mean of SPNA SST and NAO (i.e., there is little difference in the ensemble means using any randomly drawn 9 ensemble members from the ensemble mean using all 10 ensemble members; not shown). Next, we create an anomaly-hindcast with 20 ensemble members where the same CESM1-LE derived climatological ocean and sea ice ICs are used, except for full-depth salinity and temperature (EN4-Anom-Init). For these two fields, ICs are

constructed by adding EN4 (Good et al. 2013) anomalies to the CESM1-LE #34 1 November climatology. EN4 temperature and salinity anomalies are calculated from the October and November 2014 monthly means, subtracting the EN4 1954–2005 October and November mean climatology. The difference of these two hindcasts shows the influence of observation-based temperature and salinity ICs on the prediction.

d. ERAI-IC

The final hindcast set tests the effect of using atmospheric ICs derived from observations, rather than from CESM1-LE #34 restart conditions. Atmospheric ICs are derived from the ECMWF interim reanalysis [ERA-Interim (ERAI); Dee et al. 2011] and mapped to the atmospheric grid, and are the same conditions used for the NCAR-CESM contribution to the SubX project that is described in Kim et al. (2019) and Richter et al. (2020). This hindcast has 10 ensemble members and otherwise follows the CESM1-DPLE protocol.

A number of observational and reanalysis products are used for comparison to CESM1 output, including monthly mean SST from ERSSTv5 (Huang et al. 2017), monthly mean sea level pressure from HadSLP2r (Allan and Ansell 2006), and net surface heat fluxes from ERA-Interim (Dee et al. 2011). CESM1 ocean heat content and salinity are compared to those from the Met Office EN4 product (Good et al. 2013). Sea ice concentration from HadISST is used (Rayner et al. 2003). To calculate anomalies from these datasets, the same climatological period as in the drift correction (1964–2014) is employed.

To compare processes in the CESM1-FOSI to those in the CESM1-DPLE, an ocean heat budget for the upper 295 m is examined. Temperature θ tendencies for all processes are calculated online and then averaged over depth H :

$$\frac{1}{H} \int_D^{\eta} \frac{\partial \theta}{\partial t} dz = \frac{Q_{\text{net}}}{H \rho_0 C_p} + \frac{1}{H} \int_D^{\eta} [-\nabla \cdot \mathbf{u} \theta - \nabla \cdot (\mathbf{u}^* \theta + \mathbf{K})] dz, \quad (1)$$

where η is the sea surface height, D is the fixed-level depth (295 m), and $H = D + \eta$; Q_{net} is the net air–sea heat flux, ρ_0 is the model ocean reference density, and C_p is the ocean heat capacity; \mathbf{u} is the three-dimensional ocean velocity, \mathbf{u}^* is the subgrid-scale velocity from the mesoscale and submesoscale parameterizations (Gent and McWilliams 1990; Fox-Kemper et al. 2011), and \mathbf{K} is the three-dimensional diffusive temperature flux. In the analysis below, terms are grouped into four quantities as organized in the above equation: the total tendency, net surface heat fluxes, resolved advection, and subgrid-scale processes (due to both subgrid-scale velocity and diffusive fluxes) as in Yeager (2020).

The NAO index is calculated consistently across observations and CESM1 simulations. We use a pattern-based method to calculate the NAO index, rather than a station-based method, to more fully capture the behavior of the North Atlantic SLP field. Our method is similar to that used in the CESM Climate Variability and Change diagnostics package (Phillips et al. 2014) and is used for both monthly mean and DJFM-mean NAO. HadSLP2r is used for the NAO calculation rather than ERA-Interim SLP because HadSLP2r has a longer record, allowing its NAO statistics to be compared more

clearly with those from the CESM1-LE; the NAO index calculated using ERA-Interim is highly correlated with that calculated using HadSLP2r ($R = 0.97$). The seasonal cycle is removed from monthly mean HadSLP2r SLP in the North Atlantic region (90°W–40°E, 20°–80°N) from 1920 to 2018; the seasonal cycle climatology is calculated for 1964–2014 to match the drift removal method used on the CESM1-DPLE. Anomalies are normalized and weighted by $\sqrt{\cos(\phi)}$, where ϕ is latitude; CESM1-LE and CESM1-DPLE SLP output is similarly prepared then interpolated to the HadSLP2r grid. A principal component (PC) analysis is performed on the observed anomalies. The resulting empirical orthogonal functions (EOF) and PCs are then normalized by the PC standard deviations to convert the EOF pattern weights into physically meaningful units; the normalized EOF pattern magnitudes correspond to one standard deviation of the PC time series. The first normalized PC is the observed NAO index. CESM1 SLP anomalies are then projected on the observed EOF patterns; the resulting CESM1 “PCs” are normalized by the observed PC standard deviations for consistency. The first normalized CESM1 PC is the strength of the observed NAO pattern, not the model’s NAO pattern. Using the same pattern for the NAO for both observations and models allows for a cleaner comparison than does calculating EOFs individually from model output and observations. Calculating SLP EOFs separately from CESM1 output alone (rather than projecting CESM1 SLP onto observed EOFs) produces a first EOF that is very similar in pattern to its observed counterpart, but about 20% stronger in magnitude (not shown). As a result, comparison of NAO evolution using EOFs derived separately from models and observations highlights the difference in pattern magnitude, rather than any other characteristics.

3. Results

a. Comparison of the CESM1-DPLE November 2014 hindcast to observations

In this section, we examine the CESM1-DPLE hindcast initialized on 1 November 2014 and compare its evolution to observations. As discussed above, the cold blob had already developed in early 2014; as a result, the November 2014 hindcast is initialized from already cold SPNA conditions (although only half as cold as observed) and yet still fails to encompass the observed cold anomaly by more than 0.5°C during its summer 2015 peak (Figs. 3 and 4). The inability to sustain a cold anomaly for nine months in the November 2014 hindcast must be understood first, and thus earlier hindcasts that were initialized from warmer conditions are not examined. The CESM1-FOSI is used as a substitute for observations in a heat budget analysis, allowing for comparison to the same decomposition in the CESM1-DPLE. Such an analysis is not possible with observations. While the CESM1-FOSI is not a perfect reconstruction of the observed ocean, its evolution of SPNA SST during this event is similar to observations (Fig. 3a), lending some credibility to its mechanistic rendering of the cold blob. The CESM1-FOSI’s upper ocean heat content, however,

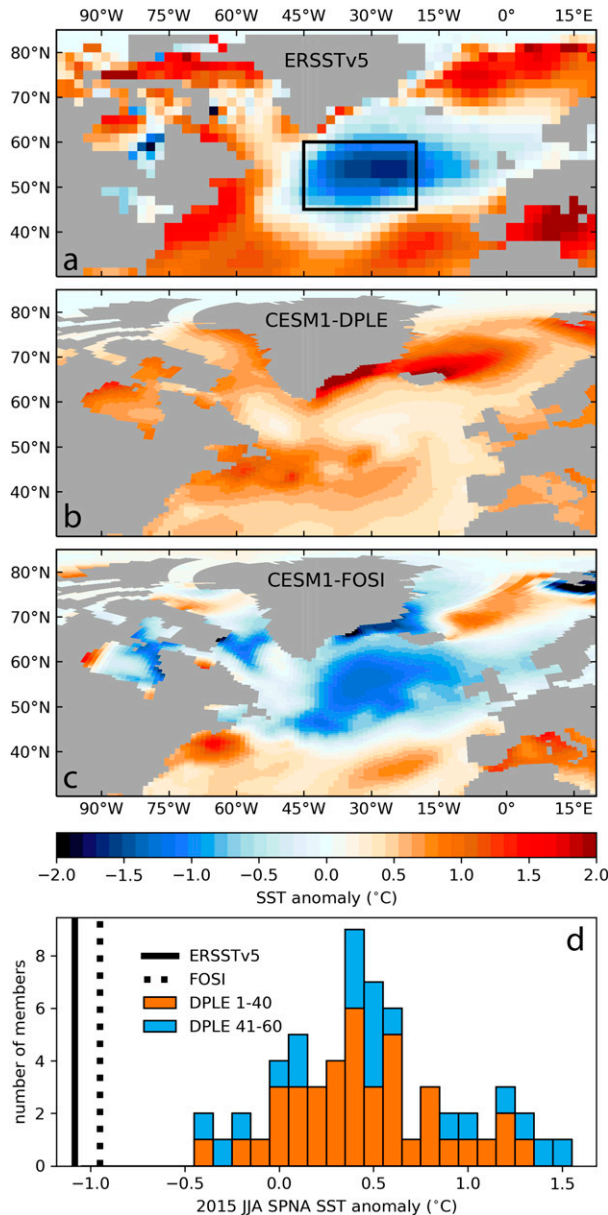


FIG. 4. The summer (JJA) 2015 cold blob in (a) ERSSTv5, (b) the CESM1-DPLE ensemble mean, and (c) CESM1-FOSI. (d) The distribution of summer SPNA SST anomalies in the original CESM1-DPLE 40 members (orange) and the additional 20-member extension (blue) is compared to the observed value (solid line) and the CESM1-FOSI value (dashed line). The box in (a) indicates the region used here to define the SPNA (45° – 20° W, 45° – 60° N).

is about half that observed, indicating that boundary forcing is able to produce a surface cold blob, but is insufficient to fully render the observed subsurface evolution (Fig. 3b). The CESM1-FOSI has negative SPNA SST anomalies throughout 2015 that are close in magnitude to observations, although the cold blob's pattern is broader than that observed (Fig. 4).

We first compare predicted and observed SPNA SST evolution from November 2014 to October 2015 (Fig. 3a).

CESM1-DPLE SPNA SST begins increasing immediately, while the observed (ERSSTv5) and CESM1-FOSI cold anomaly is sustained and later amplified. ERSSTv5 SPNA SST anomalies are more negative than those from the CESM1-FOSI, but both have similar monthly evolution. ERSSTv5 and FOSI SPNA SST are near the lower edge of the CESM1-DPLE's range through May 2015; after May 2015 both are below the CESM1-DPLE's spread. Next, SPNA volume-mean temperature in the upper 300 m is examined as a measure of OHC in both the CESM1-DPLE and FOSI because the observed cold blob also occurred subsurface (e.g., Fig. 4 in Josey et al. 2018). As with SST, the CESM1-DPLE OHC starts increasing by January 2015, which matches EN4 in January and February, but misses the strong cooling in March (Fig. 3b). Even though the CESM1-DPLE is initialized from the CESM1-FOSI, the CESM1-DPLE OHC anomaly is slightly more negative than that in the FOSI during the first month of integration. By March 2015, the EN4 OHC anomaly is well below the CESM1-DPLE's range, while the CESM1-FOSI OHC anomaly remains at the minimum edge of the DPLE range.

Next, the SPNA heat budget in the upper 300 m is compared in the CESM1-FOSI and CESM1-DPLE, as shown in Fig. 5a. The CESM1-FOSI has large monthly mean cooling tendencies in January and March 2015 (dashed black line) that are near the low edge of the CESM1-DPLE's large wintertime spread (gray shading). With 3-month running means applied (red lines and shading, Fig. 5a), the CESM1-FOSI cooling tendency falls below the CESM1-DPLE range during December 2014 and February 2015, indicating that no single ensemble member in the CESM1-DPLE had a late winter with as much total cooling as occurred in the CESM1-FOSI. Total cooling is next decomposed into the contributions from surface heat fluxes, resolved ocean advection, and subgrid-scale processes (Figs. 5b–d). In the CESM1-FOSI, cooling in January and March 2015 is due mostly to surface heat fluxes, but also has a contribution from resolved advection. A warming tendency from the subgrid-scale processes compensates the cooling from heat fluxes and advection. As with the total cooling tendency, the CESM1-DPLE range of cooling due to surface heat flux does not encompass the CESM1-FOSI's estimate of these quantities in January and March 2015. The CESM1-FOSI's cooling due to resolved advection also falls outside the CESM1-DPLE's range in March 2015. The January and March dips in the CESM1-FOSI's resolved advection term are attributable to reductions in Ekman heat transport on top of a background of negative geostrophic heat convergence (not shown). That the CESM1-FOSI's cooling occurs in two discontinuous months and is due to both surface heat fluxes and Ekman transport suggest that a relatively fast atmospheric process may be missing in the CESM1-DPLE hindcast. To examine this possibility, we next consider monthly mean surface heat fluxes and atmospheric circulation.

ERA-I surface heat flux (left column, shading) and HadSLP2r SLP (contours) anomalies from fall 2014 through spring 2015 are compared to those in the CESM1-DPLE ensemble mean (center column) in Fig. 6. The ERA-Interim surface heat flux anomalies correspond to what would be expected from atmospheric-driven turbulent heat fluxes: surface cooling is

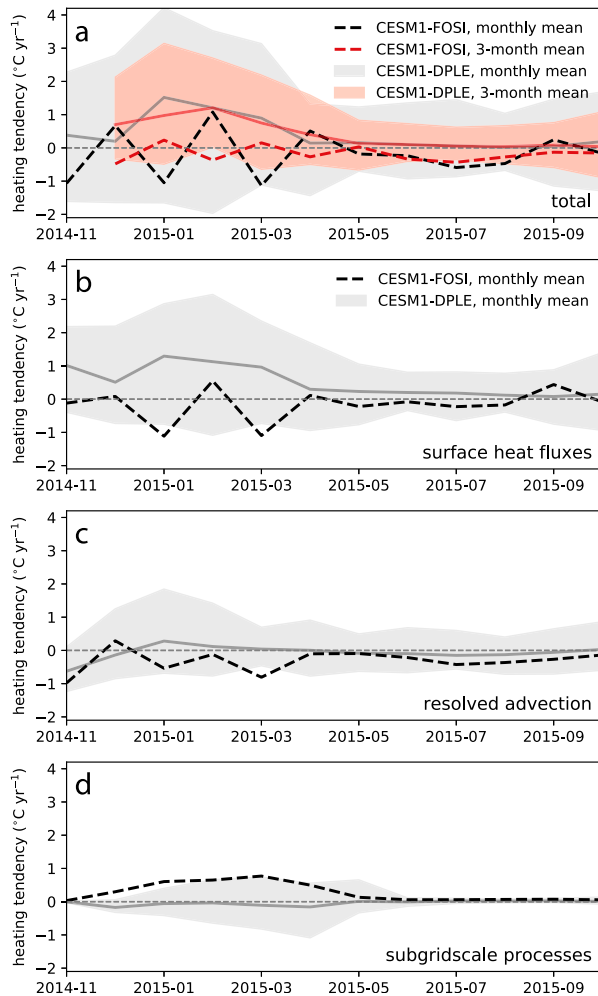


FIG. 5. SPNA heat budget analysis in the CESM1-FOSI and CESM1-DPLE. The (a) total heating tendency (positive indicates ocean warming) is decomposed into contributions from (b) surface heat fluxes, (c) resolved advection, and (d) subgrid-scale processes. Gray solid lines and gray shading indicate monthly mean CESM1-DPLE ensemble mean and range, respectively. The black dashed line indicates monthly mean CESM1-FOSI output. CESM1-DPLE and CESM1-FOSI 3-monthly running means and range are shown in red for the total tendency.

collocated with anomalously strong westerlies (as indicated by SLP gradients). The patterns of both anomalies are somewhat similar in the observation-based datasets and the ensemble mean in November 2014, although the center of low pressure and surface cooling are farther north in the CESM1-DPLE. By December though, there is no correspondence between the ensemble mean prediction and the observation-based datasets. SPNA surface cooling and an associated anomalously strong SLP gradient (i.e., anomalously strong westerlies) are present in observations especially during December 2014, January 2015, and March 2015. The CESM1-DPLE ensemble mean surface heat fluxes show the opposite: SPNA warming occurs from December onward, accompanied by near-zero SLP anomalies in the ensemble mean. In the

presence of climatological atmospheric conditions, an anomalously cold surface would result in decreased upward heat flux to the atmosphere, allowing an initially cold ocean to warm toward climatological conditions. This negative feedback of surface heat fluxes on SST appears to be the dominant mechanism at work in the CESM1-DPLE ensemble mean during winter and spring 2015. In the ensemble mean, no strong SPNA SLP gradient anomalies (strong westerlies) exist to force SPNA cooling after November 2014. The lack of strong westerlies would also weaken cooling due to decreased wind-driven ocean heat transport, especially in March. In summary, in the CESM1-DPLE ensemble mean, the atmospheric-forced cooling required to sustain the cold blob, either by turbulent heat fluxes or wind-driven transport, is absent.

The observed anomalously strong SLP gradient across the SPNA is associated with strong NAO positive conditions. As noted by Yeager et al. (2016) and Josey et al. (2018), winter 2015 was notable for its consistently strong positive NAO. The SLP anomalies from December 2014 through May 2015 project strongly on the NAO pattern (Fig. 7a): the NAO index is greater than +1 for those six consecutive months (orange line, Fig. 7b) and the DJFM NAO index during winter 2015 is the most positive of any winter in the HadSLP2r record from 1920 to 2018 (orange line, Fig. 7c). The orange columns in Fig. 7c indicate the observed NAO fraction of occurrence for each bin; the purple columns and black bars indicate the CESM1-LE NAO ensemble mean and range in each category of NAO indices, which will be discussed in the following section. In the November 2014 CESM1-DPLE hindcast, not a single ensemble member reproduces the observed stretch of positive NAO conditions or has any two months with an NAO stronger than +2, as occurred during January and March 2015, the key months for ocean cooling (Figs. 7b,c). The three ensemble members with the most positive DJFM NAO (purple lines, Fig. 7b) do, however, produce a weak cold blob in the observed location by summer 2015 (cf. Figs. 7d and 4a). Like observations, these three ensemble members also have some surface cooling to the south and east of Greenland during January through March (right column, Fig. 6).

We hypothesize that the failure of the CESM1-DPLE to sustain or deepen the SPNA cold blob in the ensemble mean and in individual ensemble members is connected to its inability to simulate the very positive NAO conditions of early 2015. In observations, positive NAO conditions that persist through winter and spring lead to ocean cooling through anomalous turbulent heat fluxes that was necessary to deepen the cold blob through spring 2015. The CESM1-DPLE has no ensemble members with DJFM NAO conditions as positive as observed. Instead, the CESM1-DPLE initial cold anomaly damps toward climatology through warming by surface fluxes. In the following section, we explore a number of hypotheses to explain why the CESM1-DPLE fails to predict both the cold blob and the positive NAO conditions.

b. Potential reasons the cold blob is not present in the CESM1-DPLE hindcast

We now explore whether CESM1 is able to reproduce the 2015 cold blob. First, can uninitialized CESM1 simulations

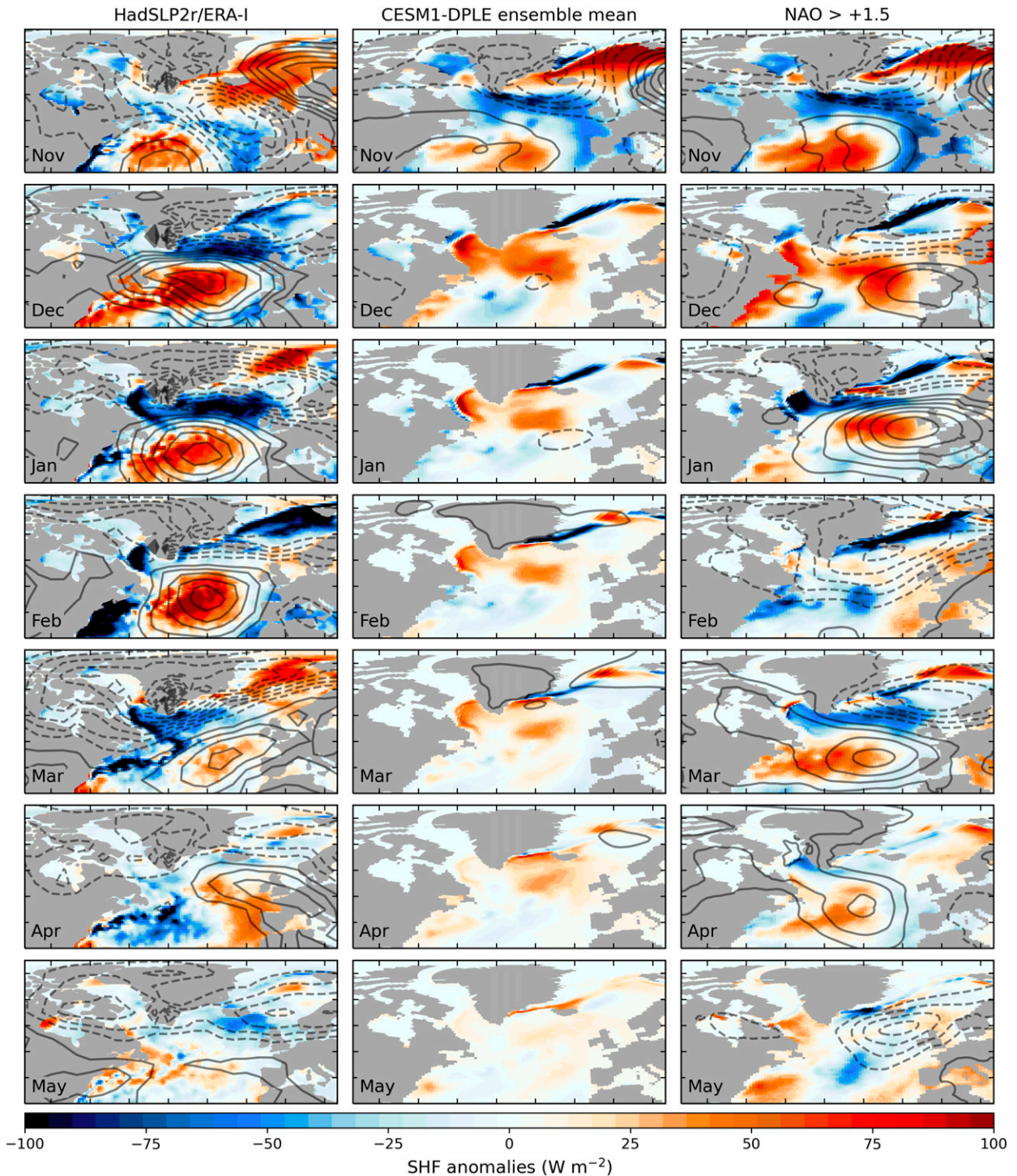


FIG. 6. Observed and predicted evolution of SLP (contours) and surface heat flux (SHF; shading) anomalies from November 2014 to May 2015. (left) Evolution of SLP and SHF anomalies from HadSLP2r and ERA-Interim, respectively, is compared against that from (center) the CESM1-DPLE ensemble mean and (right) the mean of the three CESM1-DPLE members with most positive DJFM NAO strength. Positive indicates surface heat fluxes that warm the ocean. Solid (dashed) contours indicate positive (negative) SLP anomalies and are plotted every 5 hPa with the zero contour omitted.

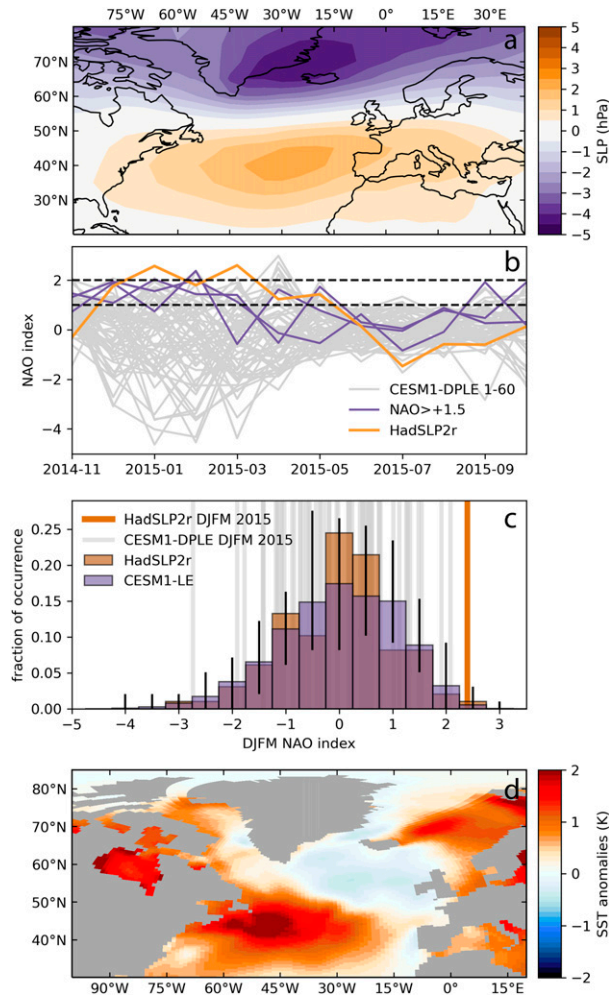


FIG. 7. (a) NAO in observations and CESM1 simulations. The monthly mean pattern for the observed NAO is derived from 1920–2018 HadSLP2r. (b) The monthly mean NAO index in HadSLP2r (orange) and all 60 CESM1-DPLE (gray; original 40 members and 20-member extension) is shown for November 2014–October 2015, where the three ensemble members with the most positive DJFM NAO index are highlighted in purple and the +1 and +2 NAO levels are indicated (dashed black lines) for context. (c) The fraction of occurrence of the DJFM NAO index in HadSLP2r from 1920–2018 (orange bars) is compared against the fraction of occurrence in the CESM1-LE ensemble mean (transparent purple bars) and its minimum and maximum range (black bars). A brown bar color is seen where the orange and purple bars overlap. For comparison, the 2015 NAO DJFM index is shown for all ensemble members of the November 2014 CESM1-DPLE hindcast (gray lines) and for HadSLP2r (orange line). (d) The mean of the three CESM1-DPLE ensemble members with most positive 2015 DJFM NAO index has a weak cold blob in the location of the observed event.

even reproduce the observed SPNA cold anomalies and positive NAO conditions? The rareness of this event has already been examined in observations in Fig. 7c. The addition of 20 members tests whether this rarity can explain the lack of a

single cold blob in the November 2014 CESM1-DPLE hindcast. Next, we conduct two targeted experiments aimed at correcting biases found in the CESM1-DPLE's November 2014 hindcast—too little B-K sea ice and a too salty and warm SPNA ocean—that could have impacted the cold blob or the NAO's evolution. The lack of B-K sea ice in the CESM1-DPLE was hypothesized to impact the NAO and cold blob based on studies suggesting that fall B-K sea ice influences springtime NAO (e.g., Li and Wang 2013; Kim et al. 2014; Screen 2017). A too salty and warm SPNA could affect the cold blob prediction simply by starting with a too warm SPNA or through incorrect stratification altering air–sea coupling. Finally, we investigate the influence of observation-based atmospheric ICs in one final hindcast set; although atmospheric ICs are not expected to strongly influence long-term ocean evolution, that expectation may not hold in this case because of the NAO's involvement.

1) SPNA EXTREME COLD AND POSITIVE NAO CONDITIONS IN CESM1

One possibility for the failure of the CESM1-DPLE to predict the 2015 cold blob is that CESM1 is unable to simulate SPNA cooling events at the observed magnitude. To test this hypothesis, the CESM1-LE is compared to observations from 1920 to 2018 of SPNA SST and NAO occurrence. We first examine annual mean SPNA SST and, given the rapid SST decline in 2014, the annual SST rate of change. Annual means are calculated from January to December of each calendar year, and are then used to calculate the annual rate of change. Anomalous SPNA SST is aggregated in 0.2°C increments and then the fraction of occurrence for each bin is calculated for both observations (ERSSTv5) and for each member of the CESM1-LE. The orange columns in Fig. 8 indicate the observed occurrence for each SPNA SST bin; annual-mean conditions as cold as in 2015 (gray line) have occurred 4% of the time in observations (4 years). The purple columns indicate the ensemble mean occurrence calculated from the histograms of all 40 CESM1-LE ensemble members. The black bars indicate the simulated range of natural variability (i.e., the lower end indicates the ensemble minimum occurrence). If the observed fraction of occurrence (orange) falls within the simulated spread of variability (black bars), the CESM1-LE and observations are consistent with each other and no pronouncements on model bias can be made. If the orange bars fall outside the range, the inconsistency between the ensemble and observations can be explained either by a model bias or by the unlikely situation where the observed occurrence of conditions was rarer than could be captured with only 40 ensemble members. For the 2015 SPNA SST annual mean anomaly, which falls in the bin ranging from -0.9° to -0.7°C , the observed fraction of occurrence is consistent with the spread of natural variability in the CESM1-LE. The ensemble also contains SPNA conditions colder than that observed in 2015; on average, SPNA SST anomalies at least as negative as observed in 2015 occur during 1.9% of all possible years in the CESM1-LE from 1920 to 2018. Results using only summer (JJA) anomalies show a similar consistency between observations and the CESM1-LE (Fig. 8b). Summer conditions as cold as

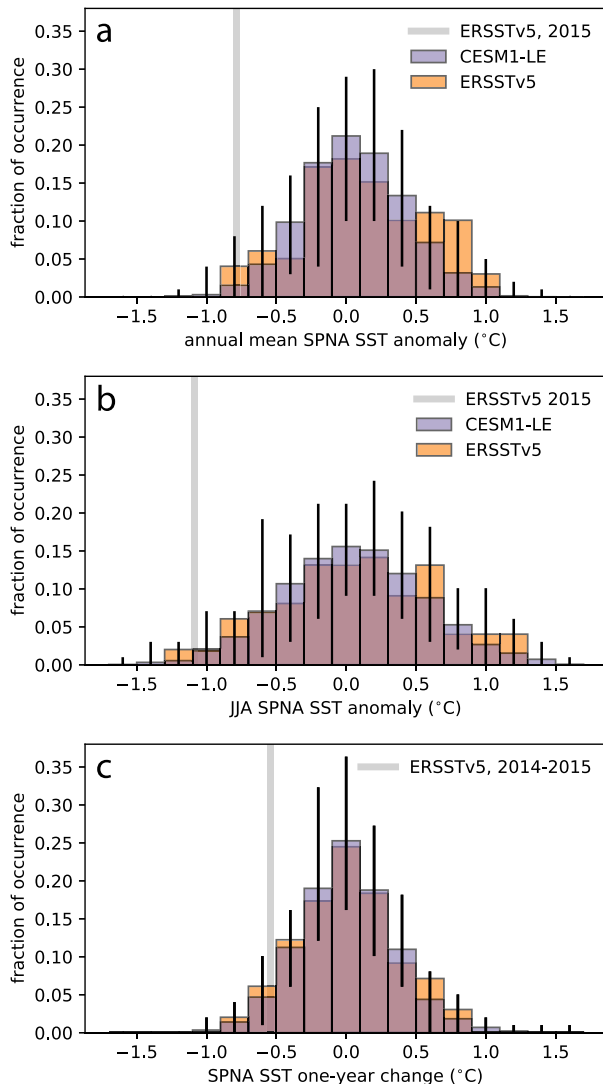


FIG. 8. Fraction of occurrence of (a) SPNA SST annual mean anomalies, (b) JJA anomalies, and (c) the 1-yr change of annual mean anomalies in the CESM1-LE (transparent purple bars) and ERSSTv5 (orange bars) from 1920 to 2018. One-year changes are calculated from annual means based on the calendar year (January–December). A brown bar color is seen where the orange and purple bars overlap. Gray lines indicate the observed value from 2015 and the 2014–15 drop. Black bars indicate the range of natural variability using the CESM1-LE’s ensemble minimum and maximum. A 1964–2014 climatology is used to calculate all anomalies.

observed occur in 1.0% of all summers from 1920 to 2018 in the entire ensemble. The CESM1-LE also simulates 1-yr drops in SPNA SST that are consistent and even larger than the decrease that occurred from 2014 to 2015 (Fig. 8c). From this cursory analysis, there is no immediate concern that CESM1 cannot simulate a cold anomaly or large declines in SPNA SST as was observed in 2015.

We next assess NAO variability in the CESM1-LE to determine if winter and spring NAO conditions as positive as

observed in 2015 (+2.4 for DJFM NAO; orange line, Fig. 7c) can be simulated in CESM1. As in the histograms of SPNA SST, Fig. 7c shows the observed (orange) and CESM1-LE (purple columns and black range bars) December–March (DJFM) mean NAO index, binned in increments of 0.5. While winters with +1 NAO index are simulated more frequently than observed, the occurrence of NAO index greater than +1.25 is consistent in observations and the CESM1-LE. The occurrence of winters with NAO index greater than or equal to +2.4 is extremely rare, occurring only once in observations from 1920 to 2018 and in only eight winters in all 40 ensemble members over the same period (0.2% of all possible winters). Depending on the ensemble member, the occurrence of such a positive NAO is 0%–2%, as compared with 1% in observations over the same time period.

It is worth noting that, although the positive winter NAO was likely a key factor in the evolution of the 2015 cold blob, SPNA cold extremes do not require positive winter NAO conditions to occur in general: SPNA heat content is not determined by surface fluxes alone. There are only weak correlations between DJFM NAO index and SPNA SST anomalies in both observations and the CESM1-LE. Using annual mean SPNA SST anomalies from ERSSTv5 and DJFM NAO calculated from HadSLP2r (1920–2018), the correlation is -0.22 , which is 90% significant; the same correlation using the full CESM1-LE during the same time period is -0.26 (95% significant). In the CESM1-LE, subsampling by positive DJFM NAO (NAO > +1.5) and low SPNA SST anomalies (SST < -0.5°C) suggests that these conditions can be associated with each other, but is not an absolute requirement (Fig. 9). Since 1980, the CESM1-LE indicates a tendency for SPNA cold events to occur only when the DJFM NAO index is near neutral or positive (dark purple markers, Fig. 9a). Likewise, since 2000, very positive DJFM NAO is associated only with near-neutral or negative SPNA SST anomaly (Fig. 9b). For both very positive NAO and very cold SPNA conditions though, there are many events in the CESM1-LE where one can occur without the other (light purple markers). In the observed record (orange markers), there are too few occurrences of both metrics (NAO index during cold events and SPNA SST anomaly during positive NAO events) to make a strong pronouncement either way. For example, there are only five SPNA cold events and two SPNA warm events that occurred with DJFM NAO > +1.5 (Fig. 9b); the occurrence of more cold events than warm ones could be due to chance.

Given the rareness of the observed SPNA SST and NAO conditions, we next examine if extending the CESM1-DPLE ensemble size increases the range of SPNA SST and NAO conditions to encompass the 2015 observations. Annual mean SPNA conditions as cold as or colder than observed in 2015 occur in about 1.9% of the years in the CESM1-LE, or roughly 1 out of every 50 years. Based on this occurrence rate in the CESM1-LE, the lack of a CESM1-DPLE cold blob could be by chance, and extending the ensemble size beyond 40 might widen the range sufficiently. To test this possibility, 20 additional CESM1-DPLE members are added to the November 2014 hindcast, which are illustrated by the blue portion of the

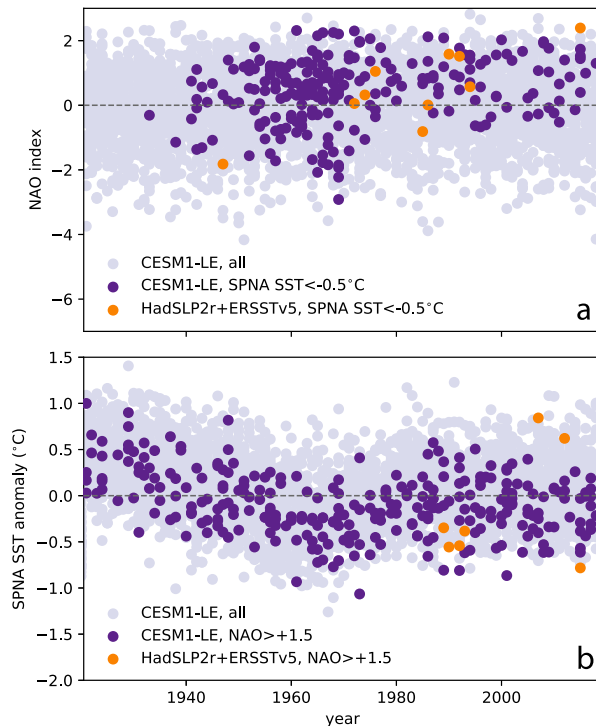


FIG. 9. Joint analysis of DJFM NAO index and SPNA SST anomaly in the CESM1-LE (purple) and observations (HadSLP2r and ERSSTv5; orange). (a) An annual mean SPNA SST anomaly of -0.5°C is used to subsample the DJFM NAO index. (b) A DJFM NAO index of $+1.5$ is used to subsample SPNA SST anomalies. A 1964–2014 climatology is used to calculate all anomalies. Subsampled CESM1-LE results are indicated by dark purple markers with the full CESM1-LE indicated by light purple markers for context.

histogram in Fig. 4d. While a few ensemble members with negative SST anomalies in summer 2015 are added, none has colder conditions than the original 40 members. The simulation of positive SST anomalies is also increased. These results suggest that something about the ICs is hindering rather than preconditioning the simulation of a summer SPNA cold anomaly.

Roughly 440 more 1-yr-long ensemble members would be required to simulate a winter NAO as positive as observed (which corresponds to an occurrence rate of 0.2%). Extending the ensemble that far is infeasible, but it is nonetheless encouraging that the 20-member extension does add a few ensemble members with relatively positive winter NAO conditions, though none as positive as observed (not shown). One of these additional positive NAO ensemble members contributes to the composite in Fig. 7d. The inability of the CESM1-DPLE to produce a single ensemble member with such positive NAO conditions could be due to the extremeness of the event making it particularly unpredictable, and the lack of a cold blob in the CESM1-DPLE may be a related result. Deficiencies in the ICs, however, also could have contributed, a possibility that we turn to next.

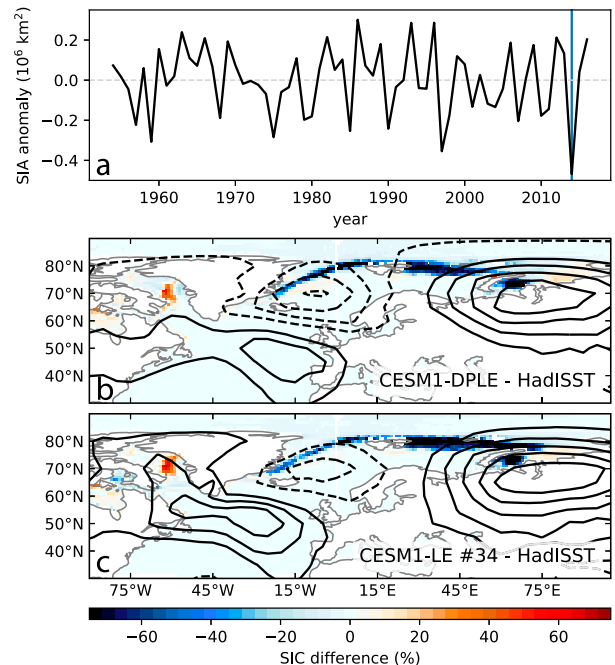


FIG. 10. CESM1-DPLE and CESM1-LE November 2014 sea ice area (SIA), sea ice concentration (SIC), and SLP difference from observations. (a) CESM1-DPLE ensemble-mean November Barents–Kara SIA difference from HadISST SIA is most negative during 2014 (blue line). (b) The CESM1-DPLE ensemble mean November-mean SIC difference from HadISST (shading) and SLP difference from HadSLP2r (contours). (c) The same differences using CESM1-LE member #34 instead of the CESM1-DPLE. Solid (dashed) contours indicate positive (negative) SLP anomalies and are plotted every 4 hPa with the zero contour omitted.

2) EVALUATING THE IMPACT OF NEW ICs

We have identified three issues with the ICs used in the November 2014 CESM1-DPLE hindcast that may have affected the simulation of North Atlantic climate in the CESM1-DPLE. The atmospheric ICs differ from observations in a way that delays fall sea ice formation; the SPNA upper ocean is too salty and not cold enough at the time of initialization, and stratospheric zonal wind anomalies have the opposite sign from observed anomalies. Each of these three issues could have individually impacted the evolution of the 2015 cold blob and NAO in the CESM1-DPLE.

First, the November B–K sea ice extent bias from observations is the most negative in the November 2014 CESM1-DPLE hindcast of all 64 hindcasts (Fig. 10a). Based on recent studies, the lack of early sea ice cover could influence the evolution of winter and spring atmospheric circulation, promoting a more negative NAO (Li and Wang 2013; Kim et al. 2014; Peings and Magnusdottir 2014; Sun et al. 2015; Screen 2017). While the low B–K sea ice anomaly in the CESM1-DPLE disappears after fall sea ice formation has completed, it is possible that the autumn sea ice state might have an influence on the late-winter NAO response in a way that winter sea ice might not. Based on lagged correlations of observed November

B-K sea ice with the subsequent winter and spring SLP (not shown), the negative sea ice anomaly could be responsible for roughly one-third of the too negative wind strength anomaly in the hindcast's winter 2015. Improving the sea ice simulation might lead to more positive NAO conditions in January and March 2015.

The negative sea ice bias is much larger in the hindcast after two weeks of integration than it is in the sea ice ICs (not shown). We instead trace the low November B-K sea ice anomaly to the atmospheric ICs from the CESM1-LE. Atmospheric ICs are drawn from restart files that were periodically saved from only one of the CESM1-LE members (#34). During November 2014, #34 exhibited an anomalously strong high centered over Siberia and a low centered northeast of Iceland that together pushed the sea ice edge northward, impeding ice formation in the B-K Seas (Fig. 10b). The anomalous November 2014 SLP and sea ice patterns in CESM1-LE #34 are uncannily similar to those in the November 2014 CESM1-DPLE ensemble mean (Fig. 10c). The day-by-day evolution of these fields in both simulations mirror each other through the third week of November, when their SLP patterns finally begin to diverge (not shown). Something about the 1 November 2014 atmospheric state in CESM1-LE #34 has particularly high predictability, which in this case affects the November sea ice formation. Similar atmospheric-driven sea ice formation delay is not seen in any of the other CESM1-DPLE hindcasts.

To test if the atmospheric ICs are responsible for the sea ice bias and, indirectly, the lack of positive winter NAO and SPNA cold blob, a 10-member hindcast is initialized on 1 November 2014 with different atmospheric ICs, referred to here as the Nov-Ice hindcast. This hindcast uses ICs from CESM1-LE member 34 on 1 November 2004. The November 2004 state from #34 has a high pressure pattern north of Iceland (which should advect ice southward and/or increase ice formation via wind-driven cooling in the B-K Seas) and it has the largest November mean B-K sea ice extent of any other year in the CESM1-LE. ICs from #34's 1 November 2004 restart should produce a more neutral or positive November sea ice anomaly. Everything else about this hindcast follows the CESM1-DPLE protocol.

November sea ice concentration is indeed improved in the B-K Seas, although it is still a bit too low outside the B-K Seas (Fig. 11). In the Nov-Ice hindcast, November SLP shows a negative NAO bias relative to observations. Despite an improvement in November sea ice simulation, by midwinter the SLP pattern indicates even weaker SPNA westerlies relative to the CESM1-DPLE—even more negative NAO conditions. In addition, the SPNA cold anomaly is lost during the first month. These results suggest that sea ice has little influence on the atmospheric circulation or the deepening of the SPNA cold blob.

The second issue is that the SPNA ocean ICs, which are from the CESM1-FOSI simulation, are not as cold or as fresh as observed from November 2014 through spring 2015 in the upper 500 m (Fig. 12). Together, these conditions translate to increased stratification in the upper 100 m in the CESM1-FOSI relative to EN4, which could indicate altered air–sea coupling through spring 2015. In the first few months of its evolution, CESM1-DPLE salinity follows the FOSI's. In the upper 50–100 m, the

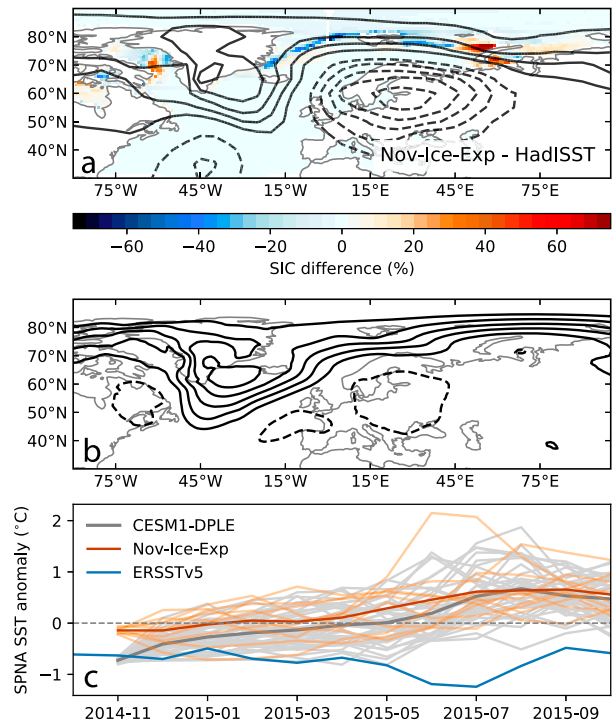


FIG. 11. SLP, SIC, and SPNA SST results of the Nov-Ice hindcast. (a) The difference of November-mean SIC between the Nov-Ice hindcast and HadISST (contours) and the difference of November-mean SLP between the hindcast and HadSLP2r (shading). The same contours/shading intervals as in Fig. 10 are used. (b) The ensemble-mean FMA SLP difference between the Nov-Ice hindcast and the CESM1-DPLE: SLP contours are every 1 hPa with the zero line omitted. (c) SPNA SST evolution in the Nov-Ice hindcast is compared to that from the CESM1-DPLE November 2014 hindcast and ERSSTv5.

CESM1-DPLE starts with a cold anomaly of $\sim 0.6^{\circ}\text{C}$ that becomes a surface-confined warm layer by summer. Under the warm layer are weakly negative temperature anomalies that are warmer than the CESM1-FOSI's. By summer 2015, very different stratification anomalies exist across these datasets that are set mostly by the strongly surface-amplified temperature anomalies. With a cold blob amplified at the surface, EN4 shows even weaker stratification (i.e., positive $d\sigma/dz$ anomaly), which the CESM1-FOSI mostly emulates due to the atmospheric boundary forcing. Without the constraining surface forcing, however, the CESM1-DPLE shows increased stratification (negative $d\sigma/dz$ anomaly), due to its anomalously warm surface conditions.

To test if ICs from the CESM1-FOSI are the cause of the CESM1-DPLE's warm SPNA during summer 2015, we next examine a hindcast initialized from EN4-derived ICs (EN4-Anom-Init). Temperature and salinity anomalies in EN4-Anom-Init are computed relative to a hindcast where the ocean and sea ice fields are initialized from CESM1-LE climatology (Climo-Init; see bottom row, Fig. 12). Through its first year of integration, the November 2014 EN4-Anom-Init ensemble mean has a SPNA that is both fresher and colder than in the CESM1-DPLE hindcast. The cold and fresh

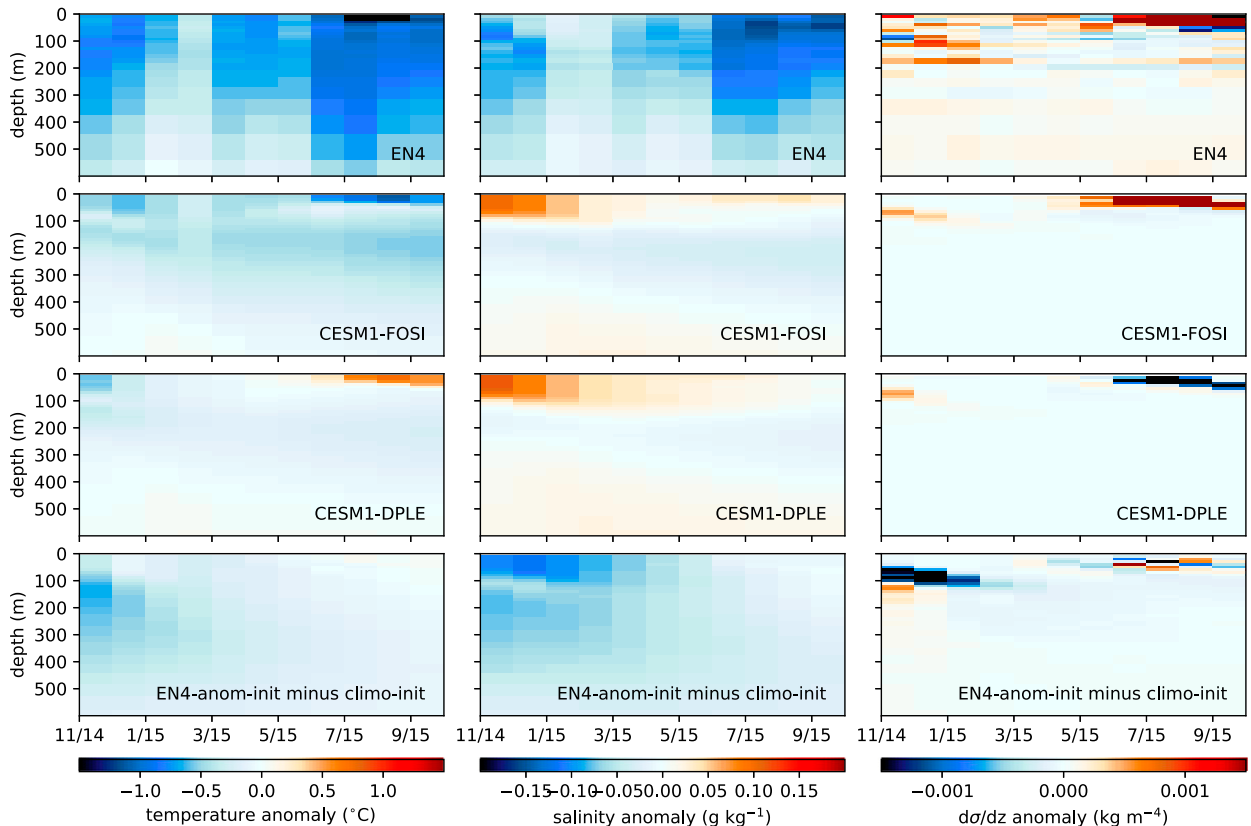


FIG. 12. Evolution of SPNA upper-600 m anomalous (left) potential temperature, (center) salinity, and (right) stratification in (first row) EN4, (second row) CESM1-FOSI, (third row) CESM1-DPLE, and (fourth row) EN4-Anom-Init hindcasts. All anomalies are calculated relative to each dataset's 1964–2014 climatology.

anomaly in the EN4-Anom-Init hindcast decays and the temperature anomaly is weaker than that in EN4. The anomaly-initialized hindcast does not have the summer warm bias that the surface CESM1-DPLE has, but it still does not have an intense cold blob as observed (Fig. 13). Interestingly, the spread in winter NAO conditions in the EN4-Anom-Init hindcast includes ensemble members with more positive conditions in January and March 2015, even though there are fewer ensemble members than in the CESM1-DPLE (Fig. 13b). These minor improvements due to fresher and colder ICs suggest that the original CESM1-DPLE ocean ICs are partly responsible for the deficiencies seen here.

Finally, we assess the influence of using atmospheric ICs derived from observed conditions. Skill of interannual-to-decadal predictions was assumed to be insensitive to atmospheric ICs because their influence is lost within weeks; this assumption was the justification for using atmospheric restart files from CESM1-LE #34 as the atmospheric ICs. For our cold blob case study, however, this assumption may not be valid, as atmospheric ICs may be key to amplifying cold SPNA conditions in the first six months. One possibility for how atmospheric ICs can affect subseasonal to seasonal (S2S) predictions is through the wintertime NAO's link to the extratropical stratospheric circulation; sudden weakening of the stratospheric westerlies, for example, can cause NAO-negative

conditions in the troposphere (see Butler et al. 2019, and references therein). S2S predictability of stratospheric polar circulation is in turn connected to tropical tropospheric phenomena (Domeisen et al. 2020). By initializing the atmosphere from CESM1-LE #34 rather than an observed source, NAO initial value predictability involving a two-way troposphere–stratospheric pathway is missing. Indeed, the CESM1-DPLE hindcast's evolution of the extratropical Northern Hemisphere stratospheric jet shows little resemblance to what was observed during winter and spring 2015. Figure 14a shows that ERA-I extratropical zonal-mean zonal wind (here measured near the latitude of maximum stratospheric jet strength, 50°–70°N) has positive anomalies that stretch from surface to stratosphere during December 2014, February 2015, and March 2015. In contrast, the CESM1-DPLE ensemble mean has consistent negative anomalies at 50 hPa (or higher) from December through March, which appear associated with weak negative tropospheric anomalies from January through March.

The ERAI-IC hindcast does not have an improved prediction of the SPNA cold blob or of the November 2014 atmospheric circulation (Figs. 14c and 15). It has a positive November 2014 mean SPNA SST anomaly, not negative as it was for the original November 2014 CESM1-DPLE hindcast and observations. This stark difference is traced to the

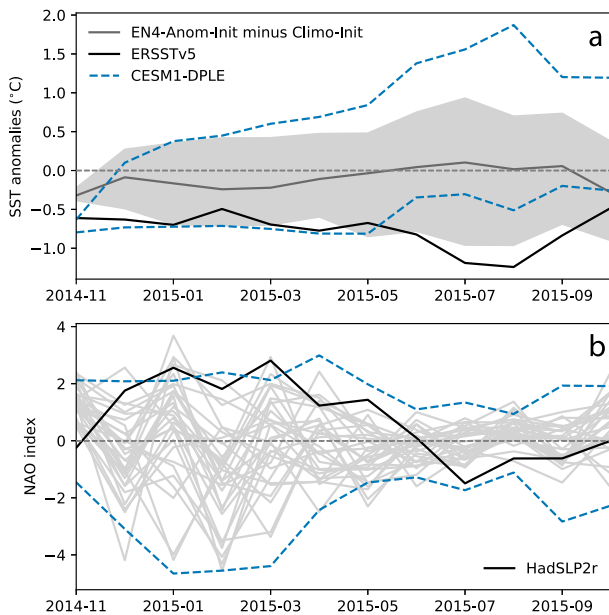


FIG. 13. (a) SPNA SST and (b) NAO evolution in the EN4-anomaly-initialized hindcast (gray) and observations (black). For reference, the minimums and maximums from the CESM1-DPLE are illustrated (blue dashed lines).

evolution of the SPNA atmosphere during the first month of the CESM1-DPLE hindcast. As described above for the Nov-Ice hindcast, the SLP pattern in the first two weeks of the CESM1-DPLE hindcast mirrors that in the CESM1-LE #34 (Figs. 10b,c). This pattern, associated with anomalously strong zonal mean winds to the south of Iceland, likely caused the negative surface heat flux anomalies through turbulent heat fluxes (Fig. 6). The persistence of the anomalously strong subpolar SLP gradient is likely behind the rapid drop in SPNA SST during the first two weeks of evolution (Fig. 15b). Part of the reason why the SPNA SST in the CESM1-DPLE is a good match with observations in November 2014 is because of the initial two-week SST drop associated with #34's unrealistic atmospheric ICs.

The evolution in the first month of the ERAI-IC hindcast is very different from that in the CESM1-DPLE. During November 2014, an anomalous high pressure centered over Greenland is associated with an anomalously strong SLP gradient in the SPNA and positive surface heat flux anomalies that warm the subpolar ocean (Fig. 15c). Like the CESM1-DPLE November SLP pattern, the atmospheric pattern has little resemblance to what was observed (Fig. 6). The anomalous surface warming is associated with a 0.4°C increase in SPNA SST during the first 30 days of integration. After only one month, the cold blob is both colder and larger in the CESM1-DPLE hindcast than in the ERAI-IC hindcast (Figs. 15d,e). One area, however, where there is an improvement in the ERAI-IC hindcast was in the Northern Hemisphere near-surface zonal-mean zonal-wind: in the 50° – 70°N latitude band, tropospheric (e.g., 1000–500 hPa) zonal wind is more positive during winter and spring 2015 (i.e., more NAO positive conditions; Fig. 14c) in the ERAI-IC hindcast than in the

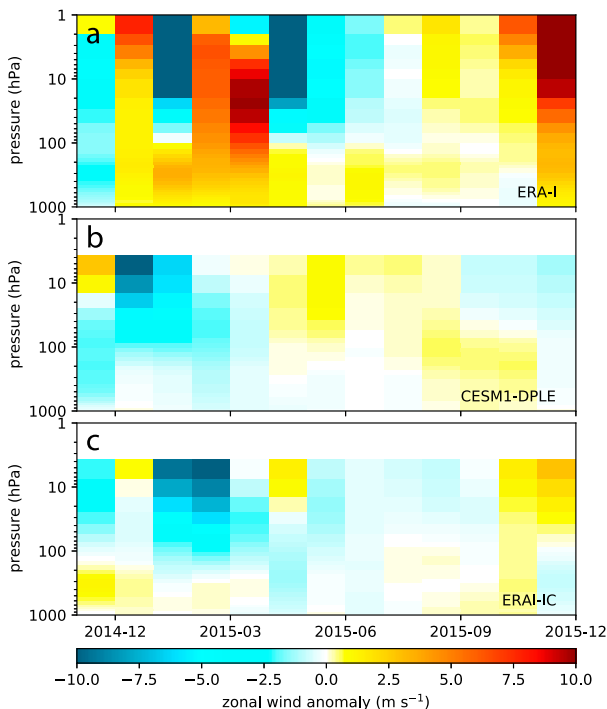


FIG. 14. Zonal-mean zonal-wind evolution at 50° – 70°N from November 2014 through December 2015 in (a) ERA-Interim (ERA-I), (b) the CESM1-DPLE ensemble mean, and (c) the ERAI-IC hindcast.

CESM1-DPLE. Beyond that one improvement though, ensemble mean zonal-mean zonal-wind in the ERAI-IC hindcast does not resemble the observed quantity more than the original CESM1-DPLE does.

4. Discussion

We have focused on two possibilities to explain why the CESM1-DPLE was unable to encompass the 2015 SPNA cold blob in its spread: that the occurrence of this event was rare and that the prediction was degraded by a deficiency in the ICs. Based on an analysis of the occurrence of SPNA SST cold events in observations and in the CESM1-LE, an ensemble size of 40 might be slightly too small to produce one cold event. Extending the CESM1-DPLE hindcast to a size of 60 still did not result in a single cold event or increase the range. While the EAP preconditioned the SPNA for a cold extreme from 2013 to 2014, positive NAO conditions during winter and spring 2015 were essential for the evolution of the cold blob. Unlike SPNA SST, the observed positive NAO conditions of 2015 were rare and unlikely to be encompassed by chance with only 60 ensemble members. The 2015 positive NAO index was a once-in-the-historic-record event in HadSLP2r, and an NAO of such magnitude occurred in only eight winters in all of the CESM1-LE's 40 members from 1920 to 2018. If the NAO's magnitude is not predictable on seasonal to interannual time scales, then the cold blob's peak magnitude—and likely the fresh blob (Holliday et al. 2020)—is also not predictable as a

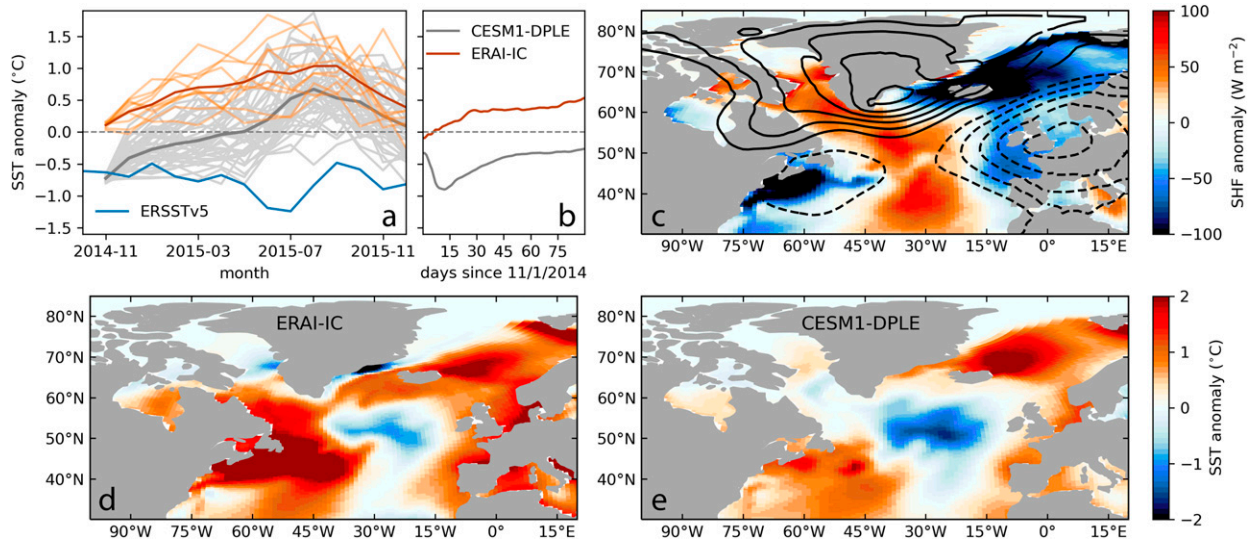


FIG. 15. Results from ERAI-IC hindcast. SPNA SST time series from the ERAI-ICs hindcast and the CESM1-DPLE are compared using both (a) monthly means and (b) daily means. (c) November 2014 monthly mean surface heat flux (shading) and SLP (contours) anomalies for the ERAI-ICs hindcast use the same contour and shading intervals as in Fig. 6. November 2014 mean SST anomalies are presented for both (d) the ERAI-ICs and (e) the CESM1-DPLE hindcasts.

result. Multiple studies, however, have shown that hindcasts initialized in November do have DJF NAO forecast skill exceeding that of a persistence forecast (Scaife et al. 2014; Kang et al. 2014; Dunstone et al. 2016; Athanasiadis et al. 2017). Beyond four months of lead time, the evidence supporting NAO predictability is varied. Kang et al. (2014) show that multiple model hindcasts initialized in November have Arctic Oscillation prediction skill that degrades by March, which, incidentally, was a key month for the 2015 cold blob's sustained cooling. In contrast, Athanasiadis et al. (2020) demonstrate that weak but statistically significant prediction skill does exist in the CESM1-DPLE for annual-mean NAO during the first lead year, with higher skill for even longer lead times. Dunstone et al. (2016) show predictable second winter NAO in the Met Office decadal prediction system (DePreSys). They identify stratospheric polar vortex strength and its link to solar forcing as key processes. These studies suggest that the NAO in general is predictable on seasonal and longer time scales, and that something about the ICs, initialization protocol, or other systematic model deficiency could explain the CESM1-DPLE's inability to predict the 2015 cold blob. The extreme NAO conditions of this particular event, however, may not have been predictable; regardless, a prediction system should be able to encompass it as a possibility.

Concerning model deficiencies, CESM1 like most CMIP-class models has a cold bias to the south of Greenland that is caused by a misplaced Gulf Stream and North Atlantic Current path (e.g., Eden et al. 2004; Weese and Bryan 2006). Because the cold bias exists in a place with large baroclinicity and at the start of the storm track, its effect on surface heat fluxes influences downstream climate and later NAO evolution through transient eddy feedbacks on the time-mean flow (Kushnir et al. 2002; Keeley et al. 2012; Drews and Greatbatch 2016). Scaife et al. (2011) show that increasing atmosphere and ocean horizontal resolution improves the cold bias and Atlantic blocking in one model. The results of Chassignet et al. (2020), however,

suggest that increased horizontal resolution is not necessarily a solution to the large surface SST biases in the SPNA. Coarse atmospheric vertical resolution and a too-low stratospheric top are other model deficiencies that could also affect the representation of the NAO and related processes (Omrani et al. 2014; Butler et al. 2016; Peings and Magnusdottir 2016; Scaife et al. 2019).

The inability to predict the NAO in this CESM1-DPLE hindcast may be a symptom of the signal-to-noise (S2N) paradox issue, where an ensemble mean prediction has higher correlation with observations than it does with any of its ensemble members (Eade et al. 2014; Scaife et al. 2014; Scaife and Smith 2018). The issue appears in multiple models, in atmosphere-only and coupled atmosphere-ocean configurations, and for a variety of climate processes, including the NAO (Smith et al. 2020). An implication is that the predictable signal's amplitude is too low relative to noise. The source of the S2N paradox has yet to be identified, although it has been suggested to be caused by deficiencies in atmospheric eddy feedbacks on the mean flow, air-sea coupling, and/or atmospheric parameterizations (Scaife and Smith 2018). The poor 2015 NAO and cold blob prediction in the CESM1-DPLE hindcast could be attributable to a too weak magnitude of a predictable NAO signal. Having statistically significant NAO correlation with observations for lead year one and longer hindcasts (Athanasiadis et al. 2020) may not be sufficient if a large NAO magnitude is necessary for the large surface fluxes required in an event such as the cold blob. Having a too weak predictable NAO signal relative to noise could also explain why the CESM1-DPLE has difficulty predicting large 1-yr SPNA SST fluctuations (Fig. 2d). If a S2N issue were partly responsible, however, extending the ensemble size should have revealed a weak but predictable NAO signal. That such a signal was not found could indicate a severe S2N problem requiring

more ensemble members than is feasible, or conversely, that a too weak NAO signal is not a cause in this case. Because the S2N issue is common across models, other decadal prediction systems may similarly struggle to predict the cold blob if a too weak NAO signal is at fault. A follow-up study using additional models will examine these possibilities.

If the CESM1-DPLE does have too weak of a predictable NAO signal, then that could explain why additional IC-based experiments here were not successful. The greatest surprise in these experiments was that the hindcast using ERA-Interim atmospheric ICs has an even warmer SPNA prediction than the original CESM1-DPLE hindcast. SPNA SST is too high starting immediately in November 2014 in the ERAI-IC hindcast, and there is little change to the atmospheric zonal mean circulation compared to the CESM1-DPLE. Ironically, the CESM1-DPLE's early match to SPNA SST observations is likely due to the incorrect atmospheric ICs from CESM1-LE #34. Part of the warming is because the cold blob is smaller in spatial extent than was observed. Using a smaller box to define the SPNA can produce a negative anomaly, though still weaker than observed. Such a cherry-picking exercise, however, ignores the observed large spatial extent of the 2015 cold blob. Regardless, that #34's ICs produce a prediction that better matches observations than observation-based ICs is surprising. While using observed atmospheric ICs in the next set of CESM decadal predictions is a logical next step, these results suggest that there may be little improvement in the SPNA, especially if a more systematic model deficiency is involved.

Anomaly initialization was implemented in CESM1 for the first time to test the influence of observed ocean ICs in a computationally cost-effective way. The initial results using anomaly-initialization show modest improvement from the original CESM1-DPLE hindcast. The EN4-Anom-Init hindcast produces an ensemble mean SPNA SST with a near-zero anomaly during summer 2015, lacking the pronounced 2015 warm overshoot in the CESM1-DPLE ensemble mean. It also features more ensemble members with negative summer SPNA SST anomalies and positive NAO conditions than in the CESM1-DPLE. Like the CESM1-DPLE, however, the EN4-Anom-Init hindcast starts losing the initial SPNA cold anomaly during the first month of evolution. Improved ocean ICs may be a way forward and it will be interesting to study the 2015 cold blob in anticipated CESM hindcasts using ICs from the Japanese 55-Year Reanalysis driving ocean–sea ice (Tsujino et al. 2018) forced FOSI.

With the benefit of hindsight, it is perhaps unsurprising that the hindcast initialized to improve November B-K sea ice formation does not have an improved winter NAO prediction. The Nov-Ice hindcast used atmospheric ICs that promote faster fall ice formation in the B-K Seas. November B-K sea ice is improved, but removing the November low pressure anomaly traced to CESM1-LE #34 also leads to an immediate November SPNA warming. Springtime midlatitude surface westerlies weaken further, the opposite of the anticipated circulation response (Fig. 11). Re-examining the literature on the influence of sea ice on atmospheric circulation suggests a few additional reasons why this hindcast had the opposite of its intended effect on the NAO. While we are able to find a statistically significant observed relationship between November Barents–Kara sea ice extent and winter and spring NAO (not

presented), the correlation was sensitive to the length of the dataset, required linear detrending, needed 3-month low-pass filtering to extract significant results, and was field significant only during February–April. With so much manipulation required to extract it, the relationship seems tenuous at best (see, e.g., Wilks 2016), an idea that is reinforced in two recent studies. Warner et al. (2020) perform the regression that we just described using the ERA-I reanalysis and HadISSTv2, and find a weakly significant relationship with low B-K sea ice extent correlated with a negative NAO-like pattern. When they perform the same regression on individual ensemble members from atmosphere-only experiments with multiple climate models, they find some ensemble members that match the observed regression pattern and others with the opposite-signed regression pattern: the observed relationship between B-K sea ice and the atmosphere's response may instead be an artifact of internal variability. Warner et al. (2020) then demonstrate that B-K sea ice and NAO responses are both independently related to La Niña, suggesting that the relationship between the two is not causal. The strength of the relationship between variability in Northern Hemisphere sea ice and atmospheric circulation is also quantified using atmosphere-only ensembles from multiple models in Liang et al. (2020). They find that only 1.5% of the total atmospheric circulation variance can be explained by variability in sea ice. In light of these results, even if a pattern of atmospheric circulation is definitively attributable to sea ice variability, it is unsurprising that atmospheric variability related to non-sea ice processes has the greater contribution in our additional hindcast.

5. Conclusions

The CESM1-DPLE skillfully predicts SPNA SST including its multidecadal time scale and encompasses the observations within its range every year, except for 2015 when the region experienced near-record cold conditions. As reported by Yeager (2020), the 2015 cold blob stands out as a high-frequency, atmospheric-forced event that took place during a period of thermohaline spindown, and that the CESM1-DPLE otherwise has a decent prediction of upper OHC cooling post-2010. The purpose of our study has been to examine what led to this prediction failure in order to illuminate directions for future CESM prediction system development. During winter and spring 2015, the amplification of the subpolar cold blob was associated with positive winter and spring NAO conditions that likely drove cooling by surface heat fluxes and ocean advection. Not a single CESM1-DPLE member has as positive NAO conditions as were observed. An examination of the CESM1-LE suggests that CESM1 simulates subpolar cold blobs with occurrence consistent with observations, but that the NAO conditions of 2015 were exceedingly rare. Deficiencies in the ICs of the ocean, atmosphere, and sea ice in the November 2014 CESM1-DPLE hindcast were identified, including too little November Barents–Kara sea ice, too warm and salty SPNA upper ocean conditions, and stratospheric zonal winds that evolved opposite to observations. Additional hindcasts were performed to test if more realistic atmosphere and ocean ICs related to these deficiencies produced better cold blob predictions. Little improvement was demonstrated, and in some hindcasts, the skill was further degraded. Using observation-derived atmospheric

ICs—low-hanging fruit for the next generation of CESM decadal predictions—is unlikely to produce great improvement on its own in the SPNA. As a particularly difficult event to predict, the 2015 cold blob case is a strong candidate for focused testing.

If CESM1 has little to no seasonal NAO predictability due to ICs, then 40 ensemble members would be far too few to encompass the 2015 NAO in its range. The extremeness of the 2015 NAO could have also made this event particularly unpredictable. An examination of the 2015 cold blob in other prediction systems, which is currently ongoing, should further illuminate if the event can be predicted and what features are associated with skill across models. We suspect that a prediction system with relatively high NAO prediction skill—whether due to model structure or initialization method—would also have a 2015 cold blob prediction that better matches observations. If, however, the amplitude of the predictable NAO signal is also too low in other models, as suggested by the generality of the S2N paradox, then this event's unpredictability may be a common finding.

Acknowledgments. This research was supported by the National Science Foundation (NSF) Collaborative Research Grant OPP-1737377. Also, this material is based upon work supported by the National Center for Atmospheric Research (NCAR), which is a major facility sponsored by the NSF under Cooperative Agreement 1852977. Portions of this study were supported by the Regional and Global Model Analysis (RGMA) component of the Earth and Environmental System Modeling Program of the U.S. Department of Energy's Office of Biological & Environmental Research (BER) via National Science Foundation IA 1947282. Support for this research was also provided by the Office of the Vice Chancellor for Research and Graduate Education at the University of Wisconsin Madison with funding from the Wisconsin Alumni Research Foundation. The anomaly-initialized hindcasts were developed after discussion with Sybren Drijfhout and Jennifer Mecking. We also acknowledge helpful conversations with Daniela Domeisen, LuAnne Thompson, and our Blue Action collaborators, and constructive feedback from three anonymous reviewers.

Data availability statement. Instructions to obtain CESM1-LE and CESM1-DPLE output are at <https://www.cesm.ucar.edu/projects/community-projects/LENS/instructions.html> and <https://www.cesm.ucar.edu/projects/community-projects/DPLE/datasets.html>, respectively. Model output from the CESM1 hindcast experiments described here are available on Zenodo at <https://doi.org/10.5281/zenodo.4050559>. Because it is infeasible to post the full output in its entirety in an online repository, only the fields presented here are included. To download or obtain all other datasets used here can be found in their respective reference documents.

REFERENCES

- Allan, R., and T. Ansell, 2006: A new globally complete monthly historical gridded mean sea level pressure dataset (HadSLP2): 1850–2004. *J. Climate*, **19**, 5816–5842, <https://doi.org/10.1175/JCLI3937.1>.
- Årthun, M., R. C. J. Wills, H. L. Johnson, L. Chafik, and H. R. Langehaug, 2021: Mechanisms of decadal North Atlantic climate variability and implications for the recent cold anomaly. *J. Climate*, **34**, 3421–3439, <https://doi.org/10.1175/JCLI-D-20-0464.1>.
- Athanasiadis, P. J., and Coauthors, 2017: A multisystem view of wintertime NAO seasonal predictions. *J. Climate*, **30**, 1461–1475, <https://doi.org/10.1175/JCLI-D-16-0153.1>.
- , S. Yeager, Y.-O. Kwon, A. Bellucci, D. W. Smith, and S. Tibaldi, 2020: Decadal predictability of North Atlantic blocking and the NAO. *npj Climate Atmos. Sci.*, **3**, 20, <https://doi.org/10.1038/s41612-020-0120-6>.
- Bellucci, A., and Coauthors, 2015: An assessment of a multi-model ensemble of decadal climate predictions. *Climate Dyn.*, **44**, 2787–2806, <https://doi.org/10.1007/s00382-014-2164-y>.
- Brady, R. X., N. S. Lovenduski, S. G. Yeager, M. C. Long, and K. Lindsay, 2020: Skillful multiyear predictions of ocean acidification in the California Current System. *Nat. Commun.*, **11**, 2166, <https://doi.org/10.1038/s41467-020-15722-x>.
- Brown, P. T., M. S. Lozier, R. Zhang, and W. Li, 2016: The necessity of cloud feedback for a basin-scale Atlantic Multidecadal Oscillation. *Geophys. Res. Lett.*, **43**, 3955–3963, <https://doi.org/10.1002/2016GL068303>.
- Butler, A. H., and Coauthors, 2016: The Climate-system Historical Forecast Project: Do stratosphere-resolving models make better seasonal climate predictions in boreal winter? *Quart. J. Roy. Meteor. Soc.*, **142**, 1413–1427, <https://doi.org/10.1002/qj.2743>.
- , and Coauthors, 2019: Sub-seasonal predictability and the stratosphere. *Sub-Seasonal to Seasonal Prediction: The Gap between Weather and Climate Forecasting*, Elsevier, 223–241, <https://doi.org/10.1016/B978-0-12-811714-9.00011-5>.
- Chassignet, E. P., and Coauthors, 2020: Impact of horizontal resolution on global ocean-sea ice model simulations based on the experimental protocols of the Ocean Model Intercomparison Project phase 2 (OMIP-2). *Geosci. Model Dev.*, **13**, 4595–4637, <https://doi.org/10.5194/gmd-13-4595-2020>.
- Chikamoto, Y., and Coauthors, 2013: An overview of decadal climate predictability in a multi-model ensemble by climate model MIROC. *Climate Dyn.*, **40**, 1201–1222, <https://doi.org/10.1007/s00382-012-1351-y>.
- Collins, M., and Coauthors, 2006: Interannual to decadal climate predictability in the North Atlantic: A multimodel-ensemble study. *J. Climate*, **19**, 1195–1203, <https://doi.org/10.1175/JCLI3654.1>.
- Compo, G. P., and Coauthors, 2011: The Twentieth Century Reanalysis Project. *Quart. J. Roy. Meteor. Soc.*, **137**, 1–28, <https://doi.org/10.1002/qj.776>.
- Curry, R. G., M. S. McCartney, and T. M. Joyce, 1998: Oceanic transport of subpolar climate signals to mid-depth subtropical waters. *Nature*, **391**, 575–577, <https://doi.org/10.1038/35356>.
- Danabasoglu, G., 2008: On multidecadal variability of the Atlantic meridional overturning circulation in the Community Climate System Model version 3. *J. Climate*, **21**, 5524–5544, <https://doi.org/10.1175/2008JCLI2019.1>.
- , S. G. Yeager, Y. O. Kwon, J. J. Tribbia, A. S. Phillips, and J. W. Hurrell, 2012: Variability of the Atlantic meridional overturning circulation in CCSM4. *J. Climate*, **25**, 5153–5172, <https://doi.org/10.1175/JCLI-D-11-00463.1>.
- , and Coauthors, 2016: North Atlantic simulations in Coordinated Ocean-ice Reference Experiments phase II (CORE-II). Part II: Inter-annual to decadal variability. *Ocean Modell.*, **97**, 65–90, <https://doi.org/10.1016/j.ocemod.2015.11.007>.
- Dee, D. P., and Coauthors, 2011: The ERA-Interim reanalysis: Configuration and performance of the data assimilation system. *Quart. J. Roy. Meteor. Soc.*, **137**, 553–597, <https://doi.org/10.1002/qj.828>.

- de Jong, M. F., and L. de Steur, 2016: Strong winter cooling over the Irminger Sea in winter 2014–2015, exceptional deep convection, and the emergence of anomalously low SST. *Geophys. Res. Lett.*, **43**, 7106–7113, <https://doi.org/10.1002/2016GL069596>.
- Delworth, T. L., and K. W. Dixon, 2000: Implications of the recent trend in the Arctic/North Atlantic oscillation for the North Atlantic thermohaline circulation. *J. Climate*, **13**, 3721–3727, [https://doi.org/10.1175/1520-0442\(2000\)013<3721:IOTRTI>2.0.CO;2](https://doi.org/10.1175/1520-0442(2000)013<3721:IOTRTI>2.0.CO;2).
- , and F. Zeng, 2016: The impact of the North Atlantic Oscillation on climate through its influence on the Atlantic meridional overturning circulation. *J. Climate*, **29**, 941–962, <https://doi.org/10.1175/JCLI-D-15-0396.1>.
- , S. Manabe, and R. J. Stouffer, 1993: Interdecadal variations of the thermohaline circulation in a coupled ocean-atmosphere model. *J. Climate*, **6**, 1993–2011, [https://doi.org/10.1175/1520-0442\(1993\)006<1993:IVOTTC>2.0.CO;2](https://doi.org/10.1175/1520-0442(1993)006<1993:IVOTTC>2.0.CO;2).
- , F. Zeng, L. Zhang, R. Zhang, G. A. Vecchi, and X. Yang, 2017: The central role of ocean dynamics in connecting the North Atlantic Oscillation to the extratropical component of the Atlantic multidecadal oscillation. *J. Climate*, **30**, 3789–3805, <https://doi.org/10.1175/JCLI-D-16-0358.1>.
- Deser, C., M. A. Alexander, S.-P. Xie, and A. S. Phillips, 2010: Sea surface temperature variability: Patterns and mechanisms. *Annu. Rev. Mar. Sci.*, **2**, 115–143, <https://doi.org/10.1146/annurev-marine-120408-151453>.
- Doblas-Reyes, F. J., and Coauthors, 2013: Initialized near-term regional climate change prediction. *Nat. Commun.*, **4**, 1715, <https://doi.org/10.1038/ncomms2704>.
- Domeisen, D. I. V., and Coauthors, 2020: The role of the stratosphere in subseasonal to seasonal prediction: 2. Predictability arising from stratosphere–troposphere coupling. *J. Geophys. Res. Atmos.*, **125**, e2019JD030923, <https://doi.org/10.1029/2019JD030923>.
- Draws, A., and R. J. Greatbatch, 2016: Atlantic multidecadal variability in a model with an improved North Atlantic current. *Geophys. Res. Lett.*, **43**, 8199–8206, <https://doi.org/10.1002/2016GL069815>.
- Drijfhout, S., G. J. van Oldenborgh, and A. Cimadoribus, 2012: Is a decline of AMOC causing the warming hole above the North Atlantic in observed and modeled warming patterns? *J. Climate*, **25**, 8373–8379, <https://doi.org/10.1175/JCLI-D-12-00490.1>.
- Duchez, A., and Coauthors, 2016: Drivers of exceptionally cold North Atlantic Ocean temperatures and their link to the 2015 European heat wave. *Environ. Res. Lett.*, **11**, 074004, <https://doi.org/10.1088/1748-9326/11/7/074004>.
- Dunstone, N., D. Smith, A. Scaife, L. Hermanson, R. Eade, N. Robinson, M. Andrews, and J. Knight, 2016: Skilful predictions of the winter North Atlantic Oscillation one year ahead. *Nat. Geosci.*, **9**, 809–814, <https://doi.org/10.1038/ngeo2824>.
- Eade, R., D. Smith, A. Scaife, E. Wallace, N. Dunstone, L. Hermanson, and N. Robinson, 2014: Do seasonal-to-decadal climate predictions underestimate the predictability of the real world? *Geophys. Res. Lett.*, **41**, 5620–5628, <https://doi.org/10.1002/2014GL061146>.
- Eden, C., and J. Willebrand, 2001: Mechanism of interannual to decadal variability of the North Atlantic circulation. *J. Climate*, **14**, 2266–2280, [https://doi.org/10.1175/1520-0442\(2001\)014<2266:MOITDV>2.0.CO;2](https://doi.org/10.1175/1520-0442(2001)014<2266:MOITDV>2.0.CO;2).
- , R. J. Greatbatch, and C. W. Böning, 2004: Adiabatically correcting an eddy-permitting model using large-scale hydrographic data: Application to the Gulf Stream and the North Atlantic Current. *J. Phys. Oceanogr.*, **34**, 701–719, [https://doi.org/10.1175/1520-0485\(2004\)034<0701:ACAEMU>2.0.CO;2](https://doi.org/10.1175/1520-0485(2004)034<0701:ACAEMU>2.0.CO;2).
- Enfield, D. B., A. M. Mestas-Núñez, and P. J. Trimble, 2001: The Atlantic Multidecadal Oscillation and its relation to rainfall and river flows in the continental U.S. *Geophys. Res. Lett.*, **28**, 2077–2080, <https://doi.org/10.1029/2000GL012745>.
- Folland, C. K., T. N. Palmer, and D. E. Parker, 1986: Sahel rainfall and worldwide sea temperatures, 1901–85. *Nature*, **320**, 602–607, <https://doi.org/10.1038/320602a0>.
- Fox-Kemper, B., and Coauthors, 2011: Parameterization of mixed layer eddies. III: Implementation and impact in global ocean climate simulations. *Ocean Modell.*, **39**, 61–78, <https://doi.org/10.1016/j.ocemod.2010.09.002>.
- García-Serrano, J., and F. J. Doblas-Reyes, 2012: On the assessment of near-surface global temperature and North Atlantic multi-decadal variability in the ENSEMBLES decadal hindcast. *Climate Dyn.*, **39**, 2025–2040, <https://doi.org/10.1007/s00382-012-1413-1>.
- Gent, P. R., and J. C. McWilliams, 1990: Isopycnal mixing in ocean circulation models. *J. Phys. Oceanogr.*, **20**, 150–155, [https://doi.org/10.1175/1520-0485\(1990\)020<0150:IMOCM>2.0.CO;2](https://doi.org/10.1175/1520-0485(1990)020<0150:IMOCM>2.0.CO;2).
- Goldenberg, S. B., C. W. Landsea, A. M. Mestas-Núñez, and W. M. Gray, 2001: The recent increase in Atlantic hurricane activity: Causes and implications. *Science*, **293**, 474–479, <https://doi.org/10.1126/science.1060040>.
- Good, S. A., M. J. Martin, and N. A. Rayner, 2013: EN4: Quality controlled ocean temperature and salinity profiles and monthly objective analyses with uncertainty estimates. *J. Geophys. Res. Oceans*, **118**, 6704–6716, <https://doi.org/10.1002/2013JC009067>.
- Griffies, S., and K. Bryan, 1997: A predictability study of simulated North Atlantic multidecadal variability. *Climate Dyn.*, **13**, 459–487, <https://doi.org/10.1007/s003820050177>.
- Grist, J. P., S. A. Josey, Z. L. Jacobs, R. Marsh, B. Sinha, and E. Van Sebille, 2016: Extreme air–sea interaction over the North Atlantic subpolar gyre during the winter of 2013–2014 and its sub-surface legacy. *Climate Dyn.*, **46**, 4027–4045, <https://doi.org/10.1007/s00382-015-2819-3>.
- Holliday, N. P., and Coauthors, 2020: Ocean circulation causes the largest freshening event for 120 years in eastern subpolar North Atlantic. *Nat. Commun.*, **11**, 585, <https://doi.org/10.1038/s41467-020-14474-y>.
- Huang, B., and Coauthors, 2017: NOAA Extended Reconstructed Sea Surface Temperature (ERSST), version 5. NOAA National Centers for Environmental Information, accessed 26 February 2019, <https://doi.org/10.7289/VST72FNM>.
- Josey, S. A., J. J.-M. Hirschi, B. Sinha, A. Duchez, J. P. Grist, and R. Marsh, 2018: The recent Atlantic cold anomaly: Causes, consequences, and related phenomena. *Annu. Rev. Mar. Sci.*, **10**, 475–501, <https://doi.org/10.1146/annurev-marine-121916-063102>.
- Kang, D., and Coauthors, 2014: Prediction of the Arctic Oscillation in boreal winter by dynamical seasonal forecasting systems. *Geophys. Res. Lett.*, **41**, 3577–3585, <https://doi.org/10.1002/2014GL060011>.
- Kay, J. E., and Coauthors, 2015: The Community Earth System Model (CESM) large ensemble project: A community resource for studying climate change in the presence of internal climate variability. *Bull. Amer. Meteor. Soc.*, **96**, 1333–1349, <https://doi.org/10.1175/BAMS-D-13-00255.1>.
- Keeley, S. P. E., R. T. Sutton, and L. C. Shaffrey, 2012: The impact of North Atlantic sea surface temperature errors on the simulation of North Atlantic European region climate. *Quart. J. Roy. Meteor. Soc.*, **138**, 1774–1783, <https://doi.org/10.1002/qj.1912>.
- Keenlyside, N. S., M. Latif, J. Jungclauss, L. Kornblueh, and E. Roeckner, 2008: Advancing decadal-scale climate prediction in the North Atlantic sector. *Nature*, **453**, 84–88, <https://doi.org/10.1038/nature06921>.

- Kim, B.-M., S.-W. Son, S.-K. Min, J.-H. Jeong, S.-J. Kim, X. Zhang, T. Shim, and J.-H. Yoon, 2014: Weakening of the stratospheric polar vortex by Arctic sea-ice loss. *Nat. Commun.*, **5**, 4646, <https://doi.org/10.1038/ncomms5646>.
- Kim, H.-M., P. J. Webster, and J. A. Curry, 2012: Evaluation of short-term climate change prediction in multi-model CMIP5 decadal hindcasts. *Geophys. Res. Lett.*, **39**, L10701, <https://doi.org/10.1029/2012GL051644>.
- , J. H. Richter, and Z. Martin, 2019: Insignificant QBO–MJO prediction skill relationship in the SubX and S2S subseasonal reforecasts. *J. Geophys. Res. Atmos.*, **124**, 12 655–12 666, <https://doi.org/10.1029/2019JD031416>.
- Kim, W. M., S. Yeager, and G. Danabasoglu, 2020: Atlantic multidecadal variability and associated climate impacts initiated by ocean thermohaline dynamics. *J. Climate*, **33**, 1317–1334, <https://doi.org/10.1175/JCLI-D-19-0530.1>.
- Kirtman, B., and Coauthors, 2013: Near-term climate change: Projections and predictability. *Climate Change 2013: The Physical Science Basis*, T. Stocker et al., Eds., Cambridge University Press, 953–1028.
- Knight, J. R., 2005: A signature of persistent natural thermohaline circulation cycles in observed climate. *Geophys. Res. Lett.*, **32**, L20708, <https://doi.org/10.1029/2005GL024233>.
- , C. K. Folland, and A. A. Scaife, 2006: Climate impacts of the Atlantic Multidecadal Oscillation. *Geophys. Res. Lett.*, **33**, L17706, <https://doi.org/10.1029/2006GL026242>.
- Kushnir, Y., W. A. Robinson, I. Bladé, N. M. Hall, S. Peng, and R. Sutton, 2002: Atmospheric GCM response to extratropical SST anomalies: Synthesis and evaluation. *J. Climate*, **15**, 2233–2256, [https://doi.org/10.1175/1520-0442\(2002\)015<2233:AGRTE>2.0.CO;2](https://doi.org/10.1175/1520-0442(2002)015<2233:AGRTE>2.0.CO;2).
- Large, W., and S. Yeager, 2009: The global climatology of an interannually varying air–sea flux data set. *Climate Dyn.*, **33**, 341–364, <https://doi.org/10.1007/s00382-008-0441-3>.
- Latif, M., and Coauthors, 2004: Reconstructing, monitoring, and predicting multidecadal-scale changes in the North Atlantic thermohaline circulation with sea surface temperature. *J. Climate*, **17**, 1605–1614, [https://doi.org/10.1175/1520-0442\(2004\)017<1605:RMAPMC>2.0.CO;2](https://doi.org/10.1175/1520-0442(2004)017<1605:RMAPMC>2.0.CO;2).
- , C. Böning, J. Willebrand, A. Biastoch, J. Dengg, N. Keenlyside, U. Schweckendiek, and G. Madec, 2006: Is the thermohaline circulation changing? *J. Climate*, **19**, 4631–4637, <https://doi.org/10.1175/JCLI3876.1>.
- Li, F., and H. Wang, 2013: Autumn sea ice cover, winter Northern Hemisphere annular mode, and winter precipitation in Eurasia. *J. Climate*, **26**, 3968–3981, <https://doi.org/10.1175/JCLI-D-12-00380.1>.
- Li, J., C. Sun, and F.-F. Jin, 2013: NAO implicated as a predictor of Northern Hemisphere mean temperature multidecadal variability. *Geophys. Res. Lett.*, **40**, 5497–5502, <https://doi.org/10.1002/2013GL057877>.
- Liang, Y., and Coauthors, 2020: Quantification of the Arctic sea ice–driven atmospheric circulation variability in coordinated large ensemble simulations. *Geophys. Res. Lett.*, **47**, e2019GL085397, <https://doi.org/10.1029/2019GL085397>.
- Lovenduski, N. S., G. B. Bonan, S. G. Yeager, K. Lindsay, and D. L. Lombardozzi, 2019: High predictability of terrestrial carbon fluxes from an initialized decadal prediction system. *Environ. Res. Lett.*, **14**, 124074, <https://doi.org/10.1088/1748-9326/ab5c55>.
- Lu, R., B. Dong, and H. Ding, 2006: Impact of the Atlantic Multidecadal Oscillation on the Asian summer monsoon. *Geophys. Res. Lett.*, **33**, L24701, <https://doi.org/10.1029/2006GL027655>.
- Marshall, J., H. Johnson, and J. Goodman, 2001: A study of the interaction of the North Atlantic Oscillation with ocean circulation. *J. Climate*, **14**, 1399–1421, [https://doi.org/10.1175/1520-0442\(2001\)014<1399:ASOTIO>2.0.CO;2](https://doi.org/10.1175/1520-0442(2001)014<1399:ASOTIO>2.0.CO;2).
- Mecking, J. V., S. S. Drijfhout, J. J.-M. Hirschi, and A. Blaker, 2019: Ocean and atmosphere influence on the 2015 European heatwave. *Environ. Res. Lett.*, **14**, 114035, <https://doi.org/10.1088/1748-9326/ab4d33>.
- Meehl, G. A., and Coauthors, 2009: Decadal prediction. *Bull. Amer. Meteor. Soc.*, **90**, 1467–1486, <https://doi.org/10.1175/2009BAMS2778.1>.
- , and Coauthors, 2014: Decadal climate prediction: An update from the trenches. *Bull. Amer. Meteor. Soc.*, **95**, 243–267, <https://doi.org/10.1175/BAMS-D-12-00241.1>.
- Msadek, R., K. W. Dixon, T. L. Delworth, and W. Hurlin, 2010: Assessing the predictability of the Atlantic meridional overturning circulation and associated fingerprints. *Geophys. Res. Lett.*, **37**, L19608, <https://doi.org/10.1029/2010GL044517>.
- , and Coauthors, 2014: Predicting a decadal shift in North Atlantic climate variability using the GFDL forecast system. *J. Climate*, **27**, 6472–6496, <https://doi.org/10.1175/JCLI-D-13-00476.1>.
- Nigam, S., A. Ruiz-Barradas, and L. Chafik, 2018: Gulf Stream excursions and sectional detachments generate the decadal pulses in the Atlantic multidecadal oscillation. *J. Climate*, **31**, 2853–2870, <https://doi.org/10.1175/JCLI-D-17-0010.1>.
- Omrani, N. E., N. S. Keenlyside, J. Bader, and E. Manzini, 2014: Stratosphere key for wintertime atmospheric response to warm Atlantic decadal conditions. *Climate Dyn.*, **42**, 649–663, <https://doi.org/10.1007/s00382-013-1860-3>.
- Peings, Y., and G. Magnusdottir, 2014: Response of the wintertime Northern Hemisphere atmospheric circulation to current and projected Arctic sea ice decline: A numerical study with CAM5. *J. Climate*, **27**, 244–264, <https://doi.org/10.1175/JCLI-D-13-00272.1>.
- , and —, 2016: Wintertime atmospheric response to Atlantic multidecadal variability: Effect of stratospheric representation and ocean–atmosphere coupling. *Climate Dyn.*, **47**, 1029–1047, <https://doi.org/10.1007/s00382-015-2887-4>.
- Phillips, A. S., C. Deser, and J. Fasullo, 2014: Evaluating modes of variability in climate models. *Eos, Trans. Amer. Geophys. Union*, **95**, 453–455, <https://doi.org/10.1002/2014EO490002>.
- Pieuch, C. G., R. M. Ponte, C. M. Little, M. W. Buckley, and I. Fukumori, 2017: Mechanisms underlying recent decadal changes in subpolar North Atlantic Ocean heat content. *J. Geophys. Res. Oceans*, **122**, 7181–7197, <https://doi.org/10.1002/2017JC012845>.
- Rahmstorf, S., J. E. Box, G. Feulner, M. E. Mann, A. Robinson, S. Rutherford, and E. J. Schaffernicht, 2015: Exceptional twentieth-century slowdown in Atlantic Ocean overturning circulation. *Nat. Climate Change*, **5**, 475–480, <https://doi.org/10.1038/nclimate2554>.
- Rayner, N. A., D. E. Parker, E. B. Horton, C. K. Folland, L. V. Alexander, D. P. Rowell, E. C. Kent, and A. Kaplan, 2003: Global analyses of sea surface temperature, sea ice, and night marine air temperature since the late nineteenth century. *J. Geophys. Res.*, **108**, 4407, <https://doi.org/10.1029/2002JD002670>.
- Richter, J. H., and Coauthors, 2020: Subseasonal prediction with and without a well-represented stratosphere in CESM1. *Weather Forecasting*, **35**, 2589–2602, <https://doi.org/10.1175/WAF-D-20-0029.1>.
- Robson, J., R. Sutton, K. Lohmann, D. Smith, and M. D. Palmer, 2012: Causes of the rapid warming of the North Atlantic

- Ocean in the mid-1990s. *J. Climate*, **25**, 4116–4134, <https://doi.org/10.1175/JCLI-D-11-00443.1>.
- , P. Ortega, and R. Sutton, 2016: A reversal of climatic trends in the North Atlantic since 2005. *Nat. Geosci.*, **9**, 513–517, <https://doi.org/10.1038/ngeo2727>.
- Scaife, A. A., and D. Smith, 2018: A signal-to-noise paradox in climate science. *npj Climate Atmos. Sci.*, **1**, 28, <https://doi.org/10.1038/s41612-018-0038-4>.
- , and Coauthors, 2011: Improved Atlantic winter blocking in a climate model. *Geophys. Res. Lett.*, **38**, L23703, <https://doi.org/10.1029/2011GL049573>.
- , and Coauthors, 2014: Skillful long-range prediction of European and North American winters. *Geophys. Res. Lett.*, **41**, 2514–2519, <https://doi.org/10.1002/2014GL059637>.
- , and Coauthors, 2019: Does increased atmospheric resolution improve seasonal climate predictions? *Atmos. Sci. Lett.*, **20**, e922, <https://doi.org/10.1002/asl.922>.
- Screen, J. A., 2017: Simulated atmospheric response to regional and pan-Arctic sea ice loss. *J. Climate*, **30**, 3945–3962, <https://doi.org/10.1175/JCLI-D-16-0197.1>.
- Smith, D. M., S. Cusack, A. W. Colman, C. K. Folland, G. R. Harris, and J. M. Murphy, 2007: Improved surface temperature prediction for the coming decade from a global climate model. *Science*, **317**, 796–799, <https://doi.org/10.1126/science.1139540>.
- , R. Eade, N. J. Dunstone, D. Fereday, J. M. Murphy, H. Pohlmann, and A. A. Scaife, 2010: Skillful multi-year predictions of Atlantic hurricane frequency. *Nat. Geosci.*, **3**, 846–849, <https://doi.org/10.1038/ngeo1004>.
- , and Coauthors, 2019: Robust skill of decadal climate predictions. *npj Climate Atmos. Sci.*, **2**, 13, <https://doi.org/10.1038/s41612-019-0071-y>.
- , and Coauthors, 2020: North Atlantic climate far more predictable than models imply. *Nature*, **583**, 796–800, <https://doi.org/10.1038/s41586-020-2525-0>.
- Sun, L., C. Deser, and R. A. Tomas, 2015: Mechanisms of stratospheric and tropospheric circulation response to projected Arctic sea ice loss. *J. Climate*, **28**, 7824–7845, <https://doi.org/10.1175/JCLI-D-15-0169.1>.
- Sutton, R. T., and B. Dong, 2012: Atlantic Ocean influence on a shift in European climate in the 1990s. *Nat. Geosci.*, **5**, 788–792, <https://doi.org/10.1038/ngeo1595>.
- Terray, L., 2012: Evidence for multiple drivers of North Atlantic multi-decadal climate variability. *Geophys. Res. Lett.*, **39**, L19712, <https://doi.org/10.1029/2012GL053046>.
- Tietsche, S., M. Balmaseda, H. Zuo, C. Roberts, M. Mayer, and L. Ferranti, 2020: The importance of North Atlantic Ocean transports for seasonal forecasts. *Climate Dyn.*, **55**, 1995–2011, <https://doi.org/10.1007/s00382-020-05364-6>.
- Tsujino, H., and Coauthors, 2018: JRA-55 based surface dataset for driving ocean–sea-ice models (JRA55-do). *Ocean Modell.*, **130**, 79–139, <https://doi.org/10.1016/j.ocemod.2018.07.002>.
- van Oldenborgh, G., F. Doblas-Reyes, B. Wouters, and W. Hazeleger, 2012: Decadal prediction skill in a multi-model ensemble. *Climate Dyn.*, **38**, 1263–1280, <https://doi.org/10.1007/s00382-012-1313-4>.
- Visbeck, M., E. P. Chassignet, R. G. Curry, T. L. Delworth, R. R. Dickson, and G. Krahmann, 2003: The ocean's response to North Atlantic Oscillation variability. *The North Atlantic Oscillation: Climatic Significance and Environmental Impact*, *Geophys. Monogr.*, Vol. 134, Amer. Geophys. Union, 113–145, <https://doi.org/10.1029/134GM06>.
- Warner, J. L., J. A. Screen, and A. A. Scaife, 2020: Links between Barents-Kara sea ice and the extratropical atmospheric circulation explained by internal variability and tropical forcing. *Geophys. Res. Lett.*, **47**, e2019GL085679, <https://doi.org/10.1029/2019GL085679>.
- Weese, S. R., and F. O. Bryan, 2006: Climate impacts of systematic errors in the simulation of the path of the North Atlantic Current. *Geophys. Res. Lett.*, **33**, L19708, <https://doi.org/10.1029/2006GL027669>.
- Wilks, D. S., 2016: “The stippling shows statistically significant grid points”: How research results are routinely overstated and overinterpreted, and what to do about it. *Bull. Amer. Meteor. Soc.*, **97**, 2263–2273, <https://doi.org/10.1175/BAMS-D-15-00267.1>.
- Wills, R. C. J., K. C. Armour, D. S. Battisti, and D. L. Hartmann, 2019: Ocean–atmosphere dynamical coupling fundamental to the Atlantic multidecadal oscillation. *J. Climate*, **32**, 251–272, <https://doi.org/10.1175/JCLI-D-18-0269.1>.
- Yeager, S., 2020: The abyssal origins of North Atlantic decadal predictability. *Climate Dyn.*, **55**, 2253–2271, <https://doi.org/10.1007/s00382-020-05382-4>.
- , and G. Danabasoglu, 2014: The origins of late-twentieth-century variations in the large-scale North Atlantic circulation. *J. Climate*, **27**, 3222–3247, <https://doi.org/10.1175/JCLI-D-13-00125.1>.
- , A. Karspeck, G. Danabasoglu, J. Tribbia, and H. Teng, 2012: A decadal prediction case study: Late twentieth-century North Atlantic ocean heat content. *J. Climate*, **25**, 5173–5189, <https://doi.org/10.1175/JCLI-D-11-00595.1>.
- , —, and —, 2015: Predicted slowdown in the rate of Atlantic sea ice loss. *Geophys. Res. Lett.*, **42**, 10704–10713, <https://doi.org/10.1002/2015GL065364>.
- , W. M. Kim, and J. Robson, 2016: What caused the Atlantic cold blob of 2015? *US CLIVAR Variations*, No. 14, U.S. CLIVAR Office, Washington, D.C., 24–31, <https://usclivar.org/newsletter/newsletters>.
- , and Coauthors, 2018: Predicting near-term changes in the Earth system: A large ensemble of initialized decadal prediction simulations using the Community Earth System Model. *Bull. Amer. Meteor. Soc.*, **99**, 1867–1886, <https://doi.org/10.1175/BAMS-D-17-0098.1>.
- Zhang, J., and R. Zhang, 2015: On the evolution of Atlantic meridional overturning circulation fingerprint and implications for decadal predictability in the North Atlantic. *Geophys. Res. Lett.*, **42**, 5419–5426, <https://doi.org/10.1002/2015GL064596>.
- Zhang, R., and T. L. Delworth, 2006: Impact of Atlantic multidecadal oscillations on India/Sahel rainfall and Atlantic hurricanes. *Geophys. Res. Lett.*, **33**, L17712, <https://doi.org/10.1029/2006GL026267>.
- , R. Sutton, G. Danabasoglu, Y.-O. Kwon, R. Marsh, S. G. Yeager, D. E. Amrhein, and C. M. Little, 2019: A review of the role of the Atlantic meridional overturning circulation in Atlantic multidecadal variability and associated climate impacts. *Rev. Geophys.*, **57**, 316–375, <https://doi.org/10.1029/2019RG000644>.